Viscoelastic and Dielectric Behavior of Entangled Blends of Linear Polyisoprenes Having Widely Separated Molecular Weights: Test of Tube Dilation Picture

Hiroshi Watanabe,* Satoshi Ishida, Yumi Matsumiya, and Tadashi Inoue

Institute for Chemical Research, Kyoto University, Uji, Kyoto 611-0011, Japan

Received August 22, 2003; Revised Manuscript Received November 10, 2003

ABSTRACT: Viscoelastic and dielectric experiments were conducted for entangled binary blends of linear *cis*-polyisoprenes (PI) having widely separated molecular weights, $M_1 = 21.4 \times 10^3 \cong 4M_e$ and $M_2 = 308 \times 10^3 \cong 62M_e$ with M_e ($\cong 5 \times 10^3$) being the entanglement molecular weight. The PI chain had type-A dipoles and its global motion (end-to-end vector fluctuation) was dielectrically active. The volume fraction of the high-M chain, v_2, was varied from 0.005 to 1. The Struglinski-Graessley parameter for the blends, $M_2M_e^2/M_1^3 = 0.79$, was larger than a threshold value $\cong$0.5 necessary for the thermal constraint release (CR) mechanism to dominate the relaxation of the dilute high-M chains. Indeed, the Rouse-like CR relaxation was experimentally detected for the blends with small $v_2 \leq 0.01$. For large v_2 ($\geq$0.05), the high-M chains were entangled with each other (as well as with the low-M chains) and exhibited solution-like relaxation behavior at long times in their terminal regime. Comparison of viscoelastic and dielectric data suggested that the molecular picture of the dynamic tube dilation (DTD; with the dilation exponent $d \cong 1.3$) incorporating the tube-edge fluctuation effect was valid in this regime. However, at intermediate times that were still longer than the relaxation time of the low-M chains, the moduli of the high-M chains were larger than the DTD prediction. In this intermediate regime, the CR equilibration of the entanglement segments in a dilated tube segment (the prerequisite of DTD) could not occur in time, thereby resulting in this failure of the DTD picture. In addition, the viscoelastic mode distribution of the high-M chains in the blends (with $v_2 \geq 0.05$) agreed with that in the corresponding solutions only in time scales longer than the time required for the CR equilibration over the whole contour of the chain. These results demonstrated the importance of the CR equilibration in the entanglement dynamics.

1. Introduction

Entanglement of long flexible chains is one of the most important subjects in the field of polymer dynamics. Binary blends of long and short chains have been serving as an important model system in this field, and a summary of previous studies can be found in recent reviews.[1,2] Those studies demonstrate that the entanglement for the long chain in the blend is (partly) loosened by a movement of the short chain. This loosening significantly affects the motion and relaxation of the long chain.

In the widely utilized tube model, the entanglement constraint for a given chain (probe) is represented as a tube surrounding the probe backbone, and the tube diameter a, being identical to the entanglement segment size, is evaluated from the entanglement plateau modulus G_N.[1−4] The above behavior of the blends unequivocally indicates that the motion of the probe is activated by the movement of the tube-forming chains. Thus, the tube model was improved by incorporating this mechanism of the probe motion/relaxation referred to as *constraint release* (CR).[1−4]

In the current tube model, a chain is considered to relax through its longitudinal motion along the tube as well as the lateral CR motion (over a distance $> a$). Description of the chain dynamics on the basis of this molecular picture requires full analysis of the motion of individual entanglement segments of the size a. However, the description can be simplified if successive β entanglement segments are mutually equilibrated through their CR motion to allow the stress to decay by a factor of $1/\beta$ in a given time scale t. For this case, those segments can be coarse-grained into an enlarged segment of a size $a' = a\beta^{1/2}$ and this enlarged segment can be utilized as the unit in description of the chain motion. Then, the chain can be modeled to relax simply through the longitudinal motion along a dilated tube of diameter a', although the mode distribution of the CR-induced stress decay is neglected in this model. This mechanism of coarse-graining, referred to as the *dynamic tube dilation* (DTD), is also incorporated in the current model.[1,2,5−10]

For a test of this DTD molecular picture, we recently focused on viscoelastic and dielectric relaxation of *cis*-polyisoprene (PI).[11−16] For the PI chains having the type-A dipoles parallel along the their backbone, the end-to-end vector fluctuation induces the dielectric relaxation. However, no fluctuation/dielectric relaxation is activated by the DTD mechanism itself, except a contribution from the chain motion at the dilated tube edge. Thus, the DTD process is differently reflected in the normalized dielectric and viscoelastic relaxation functions $\Phi(t)$ and $\mu(t)$ ($=G(t)/G_N$), the latter exhibiting the decay due to CR/DTD. This difference allowed us to formulate a specific DTD relationship between $\Phi(t)$ and $\mu(t)$ of monodisperse linear and/or star-branched type-A chains,[11,12,14,16]

$$\mu(t) = \{\Phi(t)\}^{1+d} \text{ (+ dilated tube edge effect)} \quad (1)$$

where d ($=1-1.3$) is the tube dilation exponent.

Experimental tests of eq 1 (for $d = 1$ and without tube edge effect) indicated that the DTD picture holds for the monodisperse linear chains[11,14] but fails for star chains[12−14] in the terminal regime. The failure for the

* To whom correspondence should be addressed.

10.1021/ma030443y CCC: $27.50
Published on Web 02/04/2004

star chain is attributed to its broad distribution of the motional modes: Because of this broad distribution, the dilated tube diameter a' expected for the DTD process becomes considerably large in the terminal regime and the CR equilibration over the β ($=\{a'/a\}^2$) entanglement segments, the prerequisite of the DTD picture, cannot occur in time. In contrast, for the monodisperse linear chains having narrowly distributed motional modes, a' remains rather small even in the terminal regime thereby allowing the CR equilibration to occur in time.

As suggested from these results, we should be able to examine more details of the DTD process if we could somehow tune the a' value expected for the DTD process. For the monodisperse chains explained above, the a' value and the chain motion are fully coupled and we have no easy route for this tuning. However, we may find this route for the binary blends of long and short chains, the model system utilized for establishing the CR concept and developing the DTD picture: If the long and short chains have widely separated molecular weights M_2 and M_1, the slow relaxation behavior of the long chain in the blend is similar to that in a solution having the same volume fraction v_2 of this chain.[1] The plateau modulus of this solution is proportional to $v_2^{1+\delta}$ ($\delta = 1-1.3$)[1] and the corresponding tube diameter a_{sol} scales as $v_2^{-\delta/2}$. If the DTD picture is valid, the tube in the blend should have the diameter $a' \cong a_{sol}$ at intermediate times where the short chain has fully relaxed, and the dilation exponent d in the blend would coincide with δ in the solution. This a' can be tuned through the experimentally controlled parameter, v_2. In particular, a decrease of v_2 is expected to increase the time required for the CR equilibration, thereby reducing the validity of the DTD picture.

On the basis of this idea, we have examined the viscoelastic and dielectric behavior of binary blends of linear PI chains having $M_2 \gg M_1$ as well as solutions of the high-M PI chain. Comparison of the viscoelastic and dielectric data of the blends revealed that the DTD picture for the mutually entangled high-M chains failed in a range of intermediate t and this range widened with decreasing v_2, as expected. In addition, the width of that range was consistent with the molecular picture of CR-induced DTD. Furthermore, comparison of the data for the blends and solutions indicated that the entanglement effect of the low-M chains on the motion of the high-M chain in the blends remained up to a time necessary for the CR-equilibration over the whole contour of the high-M chain. Details of these results are presented in this paper.

2. Experimental Section

2.1. Materials. A linear *cis*-polyisoprene (PI) sample was anionically synthesized with *sec*-butyllithium in heptane and characterized with GPC combined with low-angle light scattering. This sample and previously synthesized/characterized linear PI samples[11,14] were used. Molecular characteristics of these samples are summarized in Table 1. The sample code number indicates the molecular weight in units of 1000.

The systems subjected to viscoelastic and dielectric measurements were blends of high-M and low-M PI samples (L308 and L21) having various values of the L308 volume fraction v_2. The PI chains had the type-A dipoles and their global motion was clearly observed as the slow dielectric relaxation. For comparison, the monodisperse samples and solutions of L308 in a vinyl-rich oligomeric butadiene B2 (PB2000 obtained from Nisseki Co.; 1,2-vinyl:1,4-cis/trans = 83:17, $M_w \cong 2 \times 10^3$, $M_w/M_n \cong 2$)[17] were also examined. B2 was a moderately good solvent for PI.[17] Since B2 had no type-A dipoles, the slow dielectric relaxation observed for the solutions was exclusively attributed to the global motion of the L308 chain.

Table 1. Characteristics of Linear PI Samples

code	$10^{-3}M_w$	M_w/M_n
L308[a]	308	1.08
L180[a]	180	1.06
L94[b]	94.0	1.05
L21[c]	21.4	1.04

[a] Synthesized/characterized in ref 14. [b] Synthesized/characterized in ref 11. [c] Synthesized/characterized in this study.

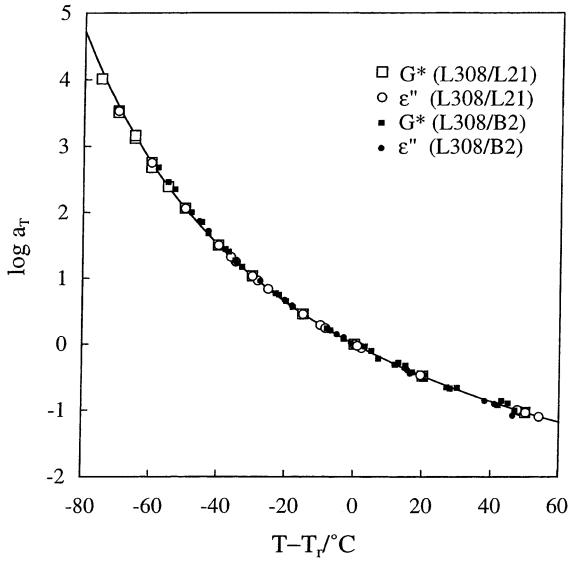

Figure 1. Shift factor a_T for the viscoelastic (G^*) and dielectric (ϵ'') data for the L308/L21 blends, monodisperse PI melts, and L308/B2 solutions. The reference temperature T_r for the iso-friction state is the same for all blends and monodisperse melts ($T_r = 40$ °C), and $T_r = 43$, 45, 47, and 48 °C for the solutions with $v_2 = 0.5$, 0.2, 0.1, and 0.05, respectively. The solid curve shows the WLF equation for the blends/monodisperse melts, $\log a_T = -4.13(T - T_r)/(150 + T - T_r)$.

Those L308/L21 blends and L308/B2 solutions were prepared by dissolving prescribed masses of L308 and L21 or B2 in benzene at ~5 wt % and then allowing benzene to thoroughly evaporate.

2.2. Measurements. 2.2.1. Methods. For the L308/L21 blends, L308/B2 solutions, and the monodisperse PI samples, dynamic viscoelastic measurements were conducted with a laboratory rheometer (ARES; Rheometrics) to determine the storage and loss moduli $G'(\omega)$ and $G''(\omega)$ at various angular frequencies ω. A parallel plate fixture of a diameter of 25 mm was utilized. The amplitude of oscillatory strain was kept small to ensure the linearity of the viscoelastic response.

For those systems charged in guarded parallel-plate dielectric cells (with the vacant capacitance of 120 and/or 80 pF), dynamic dielectric losses $\epsilon''(\omega)$ were measured with a transformer bridge (1620A, QuadTech) and a previously made circuit,[14] the latter being comprised of a function generator (WF1944, NF Corp.), an electrometer (TR8411, Advantest), and a digital recorder (DL708G, Yokogawa). The bridge was used for high-ω measurements with the usual current-compensation method,[18] and the circuit was utilized for long-time measurements with the adsorption current method. Details of the latter method were described elsewhere.[14]

2.2.2. Time−Temperature Superposition. For respective systems, the viscoelastic and dielectric data obeyed the time−temperature superposition with the same shift factor a_T. Figure 1 shows the a_T data for the L308/L21 blends and monodisperse melts (large symbols) as well as for the L308/B2 solutions (small symbols). These data are plotted against a temperature difference $T - T_r$, where T_r is the reference temperature for an iso-friction state explained below.

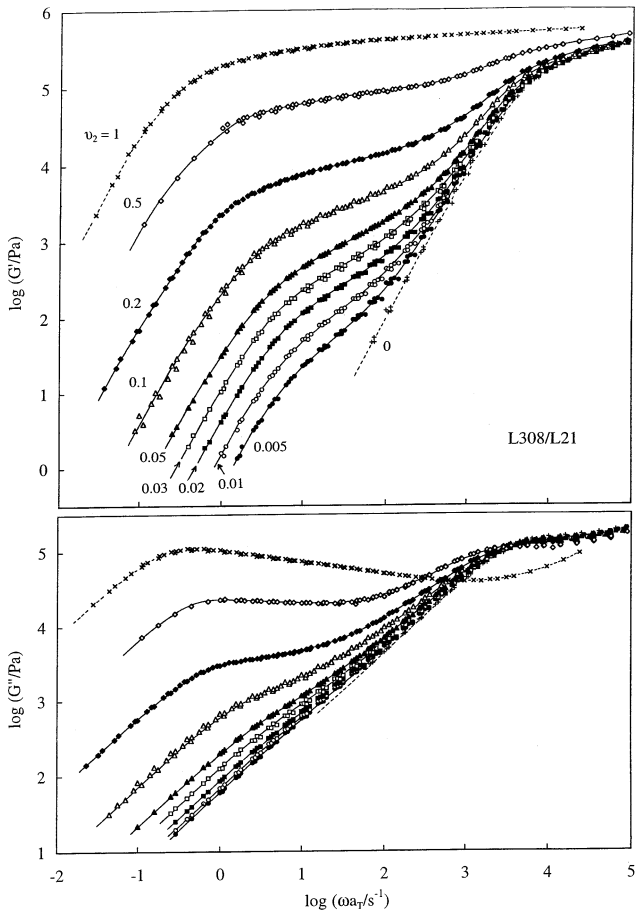

Figure 2. Storage and loss moduli G' and G'' of the L308/L21 blends in the iso-friction state at $T_r = 40$ °C. The numbers indicate the volume fraction v_2 of the high-M chain (L308).

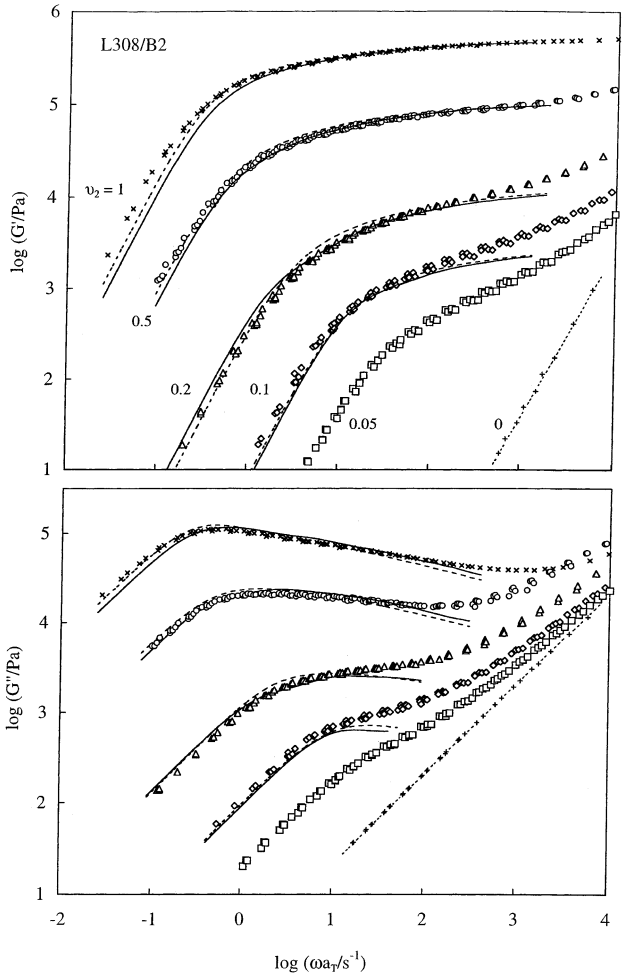

Figure 3. Storage and loss moduli G' and G'' of the L308/B2 solutions in the iso-friction state (at $T_r = 40$, 43, 45, 47, and 48 °C for $v_2 = 1$, 0.5, 0.2, 0.1, and 0.05). The data for the pure solvent (B2; $v_2 = 0$) are reduced at 48 °C (=T_r for the solution with the smallest v_2). The curves indicate the moduli calculated for the DTD process. Solid curve, for $d = 1.3$ and with the tube-edge fluctuation effect; dotted curve, for $d = 1$ and without this effect.

In the blends and monodisperse melts at a given T, the PI chains had the same monomeric friction coefficient ζ irrespective of their v_2 and M values. For these systems, we chose a reference temperature $T_r = 40$ °C. The a_T data for this T_r were well described by a WLF equation shown with the solid curve, $\log a_T = -4.13(T - T_r)/(150 + T - T_r)$. (The coefficients in this equation are very close to those obtained by Nemoto and coworkers.[19])

In contrast, in the L308/B2 solutions, ζ of the L308 chain at 40 °C changed with the L308 volume fraction v_2 because of a difference of the free volume in the neat L308 and B2 systems: B2 had a vinyl-rich microstructure and its T_g was higher than that of neat L308. Thus, we made a standard WLF analysis[20] for the a_T factor determined for ϵ'' of the solutions. (Note that the ϵ'' data exclusively reflected the PI chain motion and the a_T for those data represented changes of ζ of this chain with T.) The analysis gave $T_r = 43$, 45, 47, and 48 °C for the solutions with $v_2 = 0.5$, 0.2, 0.1, and 0.05, respectively.

As shown in Figure 1, the a_T plots for both G^* and ϵ'' of the solutions utilizing these T_r values (small symbols) are in excellent agreement with those for the blends (with $T_r = 40$ °C; large symbols). This agreement ensures that the comparison of the behavior of the blends and solutions at respective T_r is equivalent to a comparison at an iso-ζ state for the PI chains therein. In this paper, all data are reduced and compared at this iso-ζ state.

3. Results

3.1. Overview of Viscoelastic and Dielectric Data. For the L308/L21 blends and L308/B2 solutions at respective T_r, Figures 2 and 3 show the dependence of the storage and loss moduli G' and G'' on the angular frequency ω. The dielectric losses ϵ'' of these systems

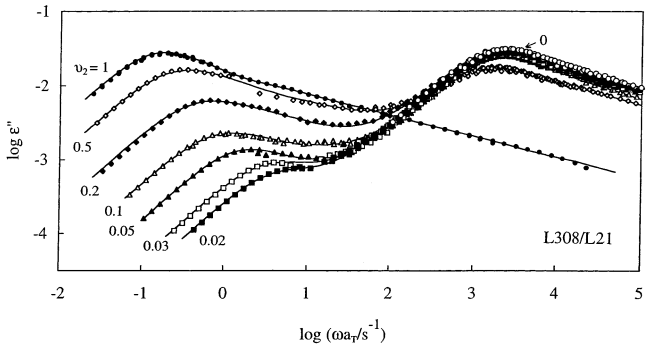

Figure 4. Dielectric loss ϵ'' of the L308/L21 blends in the iso-friction state at $T_r = 40$ °C. The numbers indicate the volume fraction v_2 of the high-M chain (L308).

are shown in Figures 4 and 5. The monomeric friction coefficient ζ of the PI chains is the same in all systems, as explained earlier (cf. Figure 1). In Figure 3, the data for $v_2 = 0$ (neat solvent B2) are reduced at T_r (=48 °C) for the solution having the smallest v_2 value (=0.05).

The L308/L21 blends exhibit two-step viscoelastic relaxation similar to that of polystyrene (PS) blends;[1] see Figure 2. The fast relaxation seen at $\omega = 10^3$–10^4

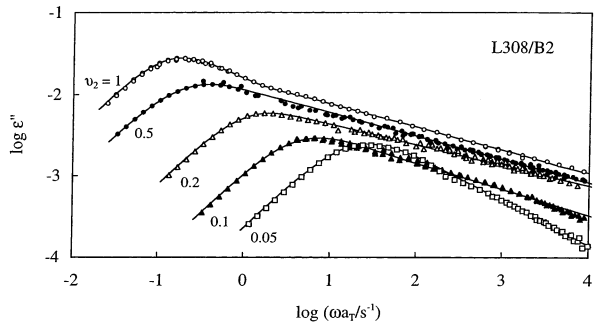

Figure 5. Dielectric loss ϵ'' of the L308/B2 solutions in the iso-friction state (at T_r = 40, 43, 45, 47, and 48 °C for υ_2 = 1, 0.5, 0.2, 0.1, and 0.05). The solvent (B2) has no type-A dipole, and the relaxation seen here is exclusively attributed to the global motion of the PI chain (L308).

s^{-1} is attributed to a full (terminal) relaxation of the low-*M* chain (L21) and a partial relaxation of the high-*M* chain (L308), while the slow relaxation at $\omega < 10^2$ s^{-1} is attributed to the full relaxation of the high-*M* chain. A similar two-step relaxation is noted for ϵ'' (Figure 4) in the same range of ω, confirming that the global motion of the high-*M* and low-*M* PI chains is dielectrically active because of their type-A dipoles. (The PI chains also have the type-B dipoles perpendicular to their backbone. However, the dielectric relaxation due to these dipoles reflects local motion of monomeric segments[15] and emerges at high ω not covered in our experiments.)

The B2 molecules have only type-B dipoles and are dielectrically inert in the range of ω examined. Thus, the L308/B2 solutions exhibit one-step dielectric relaxation exclusively attributed to the global motion of the L308 chain (Figure 5). This motion leads to the slow viscoelastic relaxation of the solution (Figure 3).

Despite the above similarity between the viscoelastic and dielectric relaxation, we also note important differences. At low $\omega < 10$ s^{-1}, the decrease of the viscoelastic loss G'' on a decrease of υ_2 to 0.1 (Figures 2 and 3) is much more significant compared to the corresponding decrease of the dielectric loss ϵ'' (Figures 4 and 5). Furthermore, a distribution of the slow viscoelastic modes significantly broadens on the decrease of υ_2 below 0.1, while a distribution of the slow dielectric modes giving the low-ω ϵ'' peak is insensitive to υ_2 for the blends (and becomes narrower for the solutions having $\upsilon_2 \leq 0.1$[21]). These differences reflect an intrinsic difference between the viscoelastic and dielectric relaxation, the former reflecting an *isochronal* orientation anisotropy of individual segments, while the latter detecting orientational correlation of these segments at two *separate* times 0 and t.[1,11−15]

Now, we compare qualitatively the relaxation behavior of the high-*M* chains in the blends and solutions. (A quantitative comparison is given later.) The ω dependence of G' and G'' is similar for the blends and solutions (cf. Figures 2 and 3). The B2 molecular weight ($M \cong 2 \times 10^3$) is well below the entanglement molecular weight of 1,2-polybutadiene ($M_e = 4 \times 10^3$)[20] and the relaxation of the high-*M* chains (L308) in the solution is affected only by their mutual entanglements. In the blends, the low-*M* chains are in a considerably entangled state ($M_1 \cong 4M_e$; $M_e = 5 \times 10^3$ for PI[22]) and the relaxation of the high-*M* chains is affected also by the entanglements with the low-*M* chains. Thus, the qualitative similarity between the blends and solutions suggests that the low-*M* chains in the blends behave as a solvent (and their entanglement effect vanishes) in the terminal regime of the blends.

This result can be related to the constraint release (CR) mechanism. A survey[1] of extensive viscoelastic data of PS/PS blends[23−29] indicated that the relaxation of the high-*M* chains in a time scale $\leq \tau_{CR,G}°$ (viscoelastic CR relaxation time for $\upsilon_2 \to 0$) is dominated by the CR mechanism when the Struglinski-Graessley parameter[30] $r_{SG} = M_2M_e^2/M_1^3$ is larger than a threshold value of $\cong$0.5:[31] namely, for $r_{SG} > 0.5$, very dilute high-*M* chains exhibit the Rouse-like CR relaxation associated with a υ_2-independent relaxation time $\langle\tau_2\rangle_G$ ($=\tau_{CR,G}°$), while $\langle\tau_2\rangle_G$ of mutually entangled high-*M* chains is larger than $\tau_{CR,G}°$ and approaches $\langle\tau_2\rangle_G$ in the solution on an increase of υ_2. PI chains would also have the threshold value of $r_{SG} \cong 0.5$, and our L308/L21 blends having $r_{SG} = 0.79$ should be in the CR dominant regime. This CR dominance naturally leads to the qualitative similarity between the L308/L21 blends and L308/B2 solutions at low ω (although a quantitative coincidence of the blend and solution behavior is noted only for large $\upsilon_2 \geq 0.5$.)

3.2. Viscoelastic Parameters of High-*M* Chain. 3.2.1. Method of Parameter Evaluation. For quantitative comparison of the viscoelastic behavior of the high-*M* chain in the blends and solutions, we need to evaluate the modulus and other viscoelastic parameters exclusively attributable to this chain.

For small υ_2, the dilute high-*M* chains in the blends do not affect the relaxation of the low-*M* chains, and this evaluation is accurately made on the basis of a blending rule formulated for the complex modulus G^* ($=G' + iG''$; $i = \sqrt{-1}$),[1,29,32]

$$G_{2,B}^*(\omega) = G_B^*(\omega) - \{1 - \upsilon_2\}G_{1,m}^*(\omega) \qquad (2)$$

Here, $G_B^*(\omega)$ and $G_{1,m}^*(\omega)$ are the moduli of the blend and the monodisperse system of the low-*M* chains, respectively, and $G_{2,B}^*(\omega)$ is the modulus of the high-*M* chains in the blend. Equation 2 simply states that the modulus of the blend is sustained by both of the high-*M* and low-*M* chains and the behavior of the low-*M* chains is the same in the monodisperse system and the blend except for a difference in their relaxation intensity (smaller in the blend by the factor of $1 - \upsilon_2$).

From eq 2, the viscosity $\eta_{2,B}$ ($=[G_{2,B}''/\omega]_{\omega\to 0}$), the elastic coefficient $A_{2,B}$ ($=[G_{2,B}'/\omega^2]_{\omega\to 0}$), and the steady-state compliance $J_{2,B}$ ($=[G_{2,B}'/\{G_{2,B}''\}^2]_{\omega\to 0}$) of the high-*M* chains in the blend are evaluated as[1,29,32]

$$\eta_{2,B} = \eta_B - (1 - \upsilon_2)\eta_{1,m},$$
$$A_{2,B} = A_B - (1 - \upsilon_2)A_{1,m},\ J_{2,B} = A_{2,B}/(\eta_{2,B})^2 \qquad (3)$$

Here, the subscripts 'B' and '1,m' stand for the data of the blend and monodisperse system of the low-*M* chains, respectively. The terminal viscoelastic relaxation time of the high-*M* chain in the blend is evaluated as[1,25,33]

$$\langle\tau_{2,B}\rangle_G = J_{2,B}\eta_{2,B} \qquad (4)$$

In the blends with large υ_2, concentrated high-*M* chains retard the motion of the low-*M* chain, as noted from the shift of the high-ω ϵ'' peak for $\upsilon_2 \geq 0.2$ (Figure 4). For this case, eq 2 is to be rewritten as $G_B^*(\omega) \cong G_{2,B}^*(\omega) + \{1 - \upsilon_2\}G_{1,m}^*(\lambda\omega)$ with λ being the retardation factor.[1,29,32] However, for large υ_2, G', and G'' at low ω are orders of magnitude larger for the blend than for

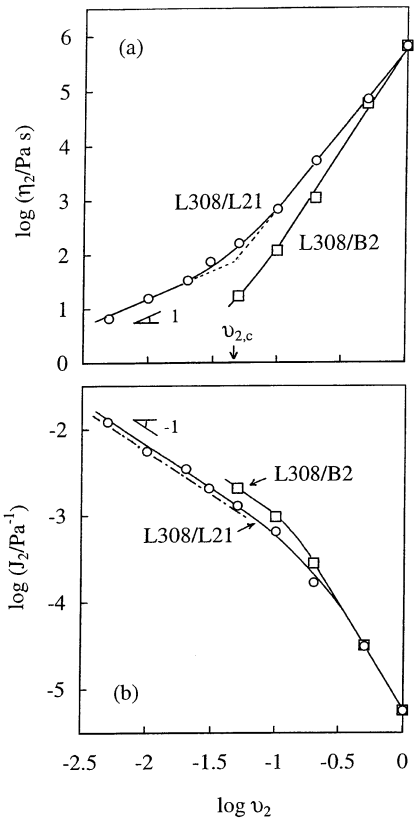

Figure 6. Viscosity η_2 and compliance J_2 of the high-*M* chain (L308) in the L308/L21 blends and L308/B2 solutions in the iso-friction state. The arrow in part a indicates the volume fraction $\upsilon_{2,c}$ for the onset of mutual entanglements of the high-*M* chains in the blend. The dash−dot line in part b shows the compliance for the Rouse CR mechanism (eq 5).

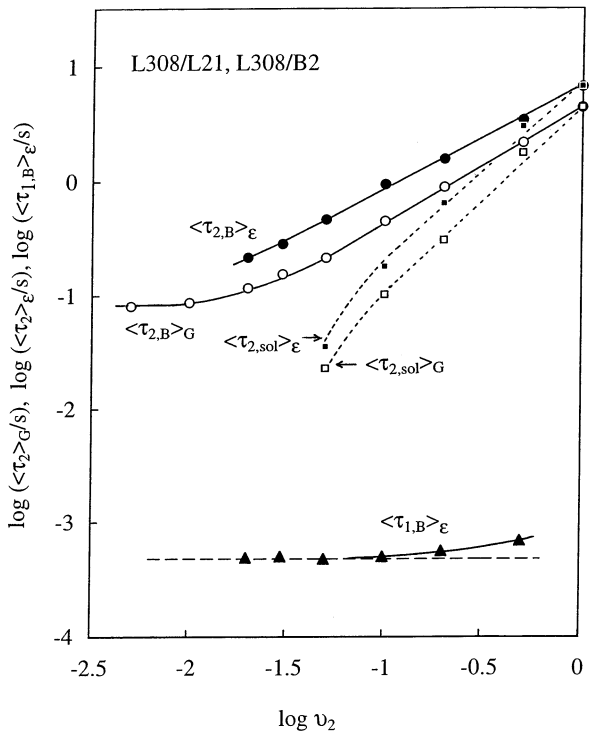

Figure 7. Viscoelastic and dielectric relaxation times (unfilled and filled symbols) of the high-*M* chain (L308) in the L308/L21 blends and L308/B2 solutions in the iso-friction state. For comparison, the dielectric relaxation time of the low-*M* chain (L21) in the blends is also shown (filled triangles).

the monodisperse low-*M* chains (cf. Figure 2) and the subtraction in eqs 2 and 3 is just a minor correction for the blend data. For this reason, we utilized eqs 3 and 4 in the entire range of υ_2 to evaluate the viscoelastic parameters of the high-*M* chains.

In the L308/B2 solution with small υ_2 (=0.05), dilute high-*M* chains negligibly affect the free volume f_{B2} for the neat B2. Then, we can apply eqs 3 and 4 to the data of the solutions and the pure solvent (B2) at T_r (= 48 °C) to evaluate $\eta_{2,sol}$, $A_{2,sol}$, $J_{2,sol}$, and $\langle\tau_{2,sol}\rangle_G$ of the high-*M* chains in this solution. In contrast, the behavior of B2 would not be exactly the same in the solutions with larger υ_2 and in its neat system at the same temperature, T_r (≤47 °C), because of a change in f_{B2} due to L308. However, B2 hardly contributes to the G^* of the solutions at low ω, and the subtraction in eqs 2 and 3 (with the subscript '1,m' standing for B2) is again minor. Thus, in the entire range of υ_2, we applied eqs 3 and 4 to the data of the solutions and B2 at T_r to evaluate the parameters for the high-*M* chains in the solutions.

3.2.2. υ_2 dependence of viscoelastic parameters. For the high-*M* chains in the blends and solutions, the η_2 and J_2 data obtained with the above method are summarized in Figure 6, and the viscoelastic relaxation time $\langle\tau_2\rangle_G$ is shown with the unfilled symbols in Figure 7. (Filled symbols denote the dielectric relaxation time explained later.) These data were determined in the iso-friction state at T_r.

In the blends with small υ_2, $\eta_{2,B}$ and $J_{2,B}$ of the high-*M* chain are proportional to υ_2 and υ_2^{-1}, respectively; see circles in Figure 6. Furthermore, the $J_{2,B}$ value is close to the Rouse value indicated with the dash−dot line in part b,

$$J_{\text{Rouse}} = \frac{2M_2}{5c_2RT} \tag{5}$$

Here, c_2 is the high-*M* chain concentration (in mass/volume unit), T is the absolute temperature, and R is the gas constant. These features are characteristic to dilute high-*M* chains that fully relax through the Rouse-like CR process.[1,29,32]

For large υ_2, $J_{2,B}$ and $\eta_{2,B}$ depend more strongly on υ_2 and gradually approach $J_{2,sol}$ and $\eta_{2,sol}$ of the high-*M* chain in the solutions (squares). The data of these entangled solutions exhibit the well-known, power-law type υ_2 dependence (at the iso-friction state),

$$J_{2,\text{sol}} \propto \upsilon_2^{-\alpha} \quad \text{with } \alpha = 2.2-2.3 \tag{6a}$$

$$\eta_{2,\text{sol}} \propto \upsilon_2^{\alpha'} \quad \text{with } \alpha' = 3.6-3.7 \tag{6b}$$

Thus, the relaxation of the high-*M* chain in the blends exhibits a crossover from the dilute regime (where $\eta_{2,B} \propto \upsilon_2$ and $J_{2,B} \propto \upsilon_2^{-1}$) to the concentrated regime (where $\eta_{2,B}$ and $J_{2,B}$ approach the solution data). A characteristic volume fraction $\upsilon_{2,c}$ for this crossover was evaluated from a crossing point of the asymptotic lines for the $\eta_{2,B}$ data in these two regimes (dotted lines in Figure 6a). The result was

$$\upsilon_{2,c} = 0.046 \pm 0.004 \tag{7}$$

This $\upsilon_{2,c}$ value is utilized in our later discussion of the DTD picture.

In Figure 6, we also note that $\eta_{2,B}$ is significantly larger than $\eta_{2,sol}$ in a range $\upsilon_2 \leq 0.2$ and the close coincidence of $\eta_{2,B}$ and $\eta_{2,sol}$ is observed only for larger υ_2 (=0.5). In contrast, $J_{2,B}$ is not significantly different from $J_{2,sol}$ even for $\upsilon_2 \leq 0.2$. The compliance $J_{2,B}$ is sensitive to the distribution of the terminal viscoelastic modes of the high-M chain but independent of the value of the relaxation time $\langle\tau_{2,B}\rangle_G$, while the viscosity $\eta_{2,B}$ ($=\langle\tau_{2,B}\rangle_G/J_{2,B}$; eq 4) is affected by both mode distribution and relaxation time. Thus, the difference between $\eta_{2,B}$ and $J_{2,B}$ indicates that the concentrated high-M chains in the blends exhibit the terminal mode distribution similar to that in the solutions but its relaxation is retarded by the low-M chain (as confirmed from direct comparison of $\langle\tau_{2,B}\rangle_G$ and $\langle\tau_{2,sol}\rangle_G$ in Figure 7). In other words, for $\upsilon_2 \leq 0.2$ the low-M chain has fully relaxed at $t \ll \langle\tau_{2,B}\rangle_G$ but its entanglement effect on the motion of the high-M chain vanishes only at much longer t (close to $\langle\tau_{2,B}\rangle_G$). This long-lived entanglement effect is further discussed later in relation to the CR equilibration.

Now, we turn our attention to the relaxation times $\langle\tau_{2,B}\rangle_G$ and $\langle\tau_{2,sol}\rangle_G$ shown in Figure 7. In the concentrated solutions, $\langle\tau_{2,sol}\rangle_G$ ($=J_{2,sol}\eta_{2,sol}$) exhibits the power-law type υ_2 dependence corresponding to eq 6; see unfilled squares. The $\langle\tau_{2,B}\rangle_G$ in the blend (unfilled circles) gradually approaches $\langle\tau_{2,sol}\rangle_G$ with increasing υ_2, but a considerable difference remains until υ_2 is increased to 0.5. This difference reflects the long-lived entanglement effect due to the low-M chains in the blend.

Figure 7 also demonstrates that $\langle\tau_{2,B}\rangle_G$ becomes independent of υ_2 at sufficiently small $\upsilon_2 \leq 0.01$ (well below $\upsilon_{2,c}$; cf. eq 7). Since our blends have a large Struglinski-Graessley parameter, $r_{SG} = M_2M_e^2/M_1^3 = 0.79$, the high-$M$ chain in this dilute limit should fully relax through the Rouse-like CR process. (This assignment is consistent with the close coincidence of $J_{2,B}$ and J_{Rouse} seen in Figure 6b.) Thus, the $\langle\tau_{2,B}\rangle_G$ (=0.081 s) for $\upsilon_2 \leq 0.01$ can be utilized as the viscoelastic CR relaxation time in the dilute limit, $\tau_{CR,G}°$. The viscoelastic relaxation reflects the relaxation of isochronal orientation anisotropy and is faster, by a factor of 2, than the CR equilibration of the entanglement segments (which corresponds to the dielectric relaxation).[1,15] Considering this point, we evaluated the time required for the CR equilibration of all entanglement segments of the high-M chain as

$$\tau_{CR,\epsilon}° = 2\tau_{CR,G}° = 0.16 \text{ s} \quad (8)$$

This $\tau_{CR,\epsilon}°$ becomes the key in our later discussion of the DTD picture.

3.3. Reduced Plots of G' and G''. The entanglement plateau modulus G_{N2} due only to the mutually entangled high-M chains plays an essential role in the DTD molecular picture. For an experimental test of the υ_2 dependence of G_{N2}, we reduced the G' and G'' data by a factor of υ_2^{1+d} (d = dilation exponent) and plotted these reduced moduli against a normalized frequency $\omega\langle\tau_{2,B}\rangle_G$. Here, $\langle\tau_{2,B}\rangle_G$ is the terminal viscoelastic relaxation time of the high-M chain summarized in Figure 7 (unfilled circles). For the L308/ L21 blends with various υ_2, Figure 8 compares the reduced plots with $d = 1.3$. For the L308/B2 solutions, similar plots utilizing the $\langle\tau_{2,sol}\rangle_G$ data (Figure 7) are shown in Figure 9.

G' is much less sensitive to the fast relaxation modes compared to G''. For both blends and solutions having $\upsilon_2 \geq 0.1$, excellent superposition is observed for the reduced plots of G' at low ω; see top panels in Figures 8 and 9. A similar quality of superposition is achieved for G'' in a range of $\upsilon_2 \geq 0.2$, and the deviation seen for $\upsilon_2 = 0.1$ is mainly due to the contribution from the fast relaxation of the low-M chains/solvent B2 (as well as the fast, partial relaxation of the high-M chain). These results indicate that the high-M chains in the blends and/or solutions with $\upsilon_2 \geq 0.1$ exhibit the universal distribution of slow viscoelastic modes (in the reduced scale) governed by the same type of relaxation mechanism and that the dilation exponent for the blends is close to $d = 1.3$. This d is close to the exponent $d = 4/3$ theoretically suggested by Colby and Rubinstein.[34] (Park and Larson[35] compared the viscoelastic data for monodisperse star 1,4-polybutadiene (PB) with the DTD model[7,8] to conclude $d = 4/3$ for PB systems.)

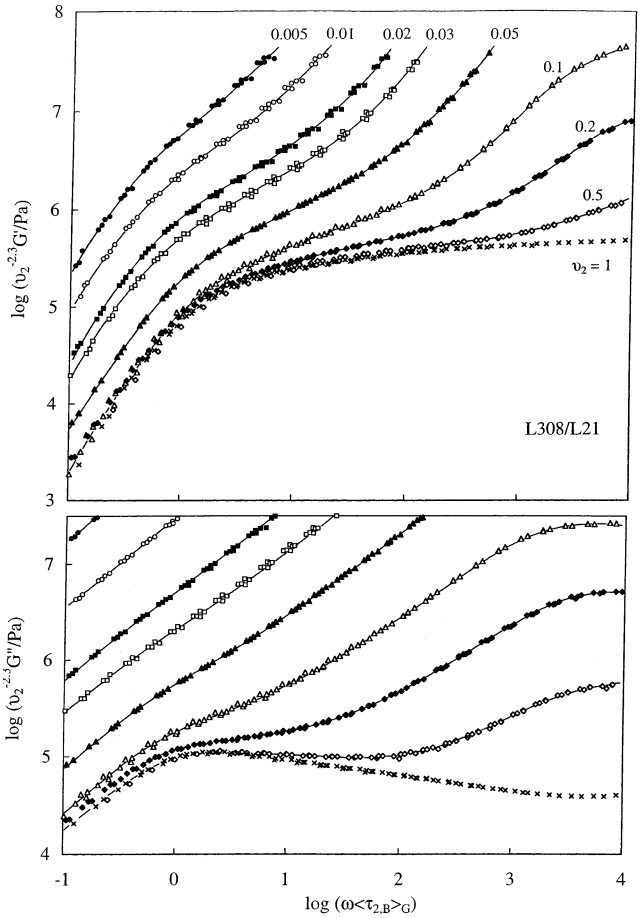

Figure 8. Plots of reduced moduli $\upsilon_2^{-2.3}G'$ and $\upsilon_2^{-2.3}G''$ of the L308/L21 blends against the normalized frequency $\omega\langle\tau_{2,B}\rangle_G$. The terminal viscoelastic relaxation time of the high-M chain (L308) in the blends, $\langle\tau_{2,B}\rangle_G$, is given in Figure 7.

In relation to this result, we should emphasize that the superposition failed for the simplest exponent of $d = 1$. For the L308/L21 blends, this failure is demonstrated in Figure 10 where $\upsilon_2^{-2}G'$ and $\upsilon_2^{-2}G''$ are plotted against $\omega\langle\tau_{2,B}\rangle_G$; see the scatter of the plots at $\omega\langle\tau_{2,B}\rangle_G < 10$. Although not shown here, a similar magnitude of failure for $d = 1$ was confirmed for the L308/B2 solutions. (However, $d = 1$ was successfully applied to the monodisperse linear PI chains examined in our previous studies.[11,14,15] An explanation about this success is given at the end of this paper.)

The above results unequivocally demonstrate that the dilation exponent for our PI systems (giving the scaling $G_{N2} \propto \upsilon_2^{1+d}$) is considerably larger than 1 and close to

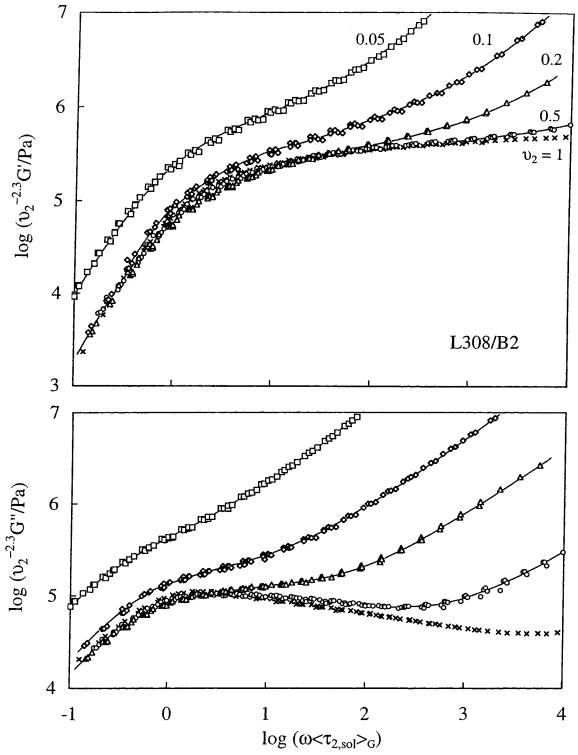

Figure 9. Plots of reduced moduli $\upsilon_2^{-2.3}G'$ and $\upsilon_2^{-2.3}G''$ of the L308/B2 solutions against the normalized frequency $\omega\langle\tau_{2,sol}\rangle_G$. The terminal viscoelastic relaxation time of the high-M chain (L308) in the solutions, $\langle\tau_{2,sol}\rangle_G$, is given in Figure 7.

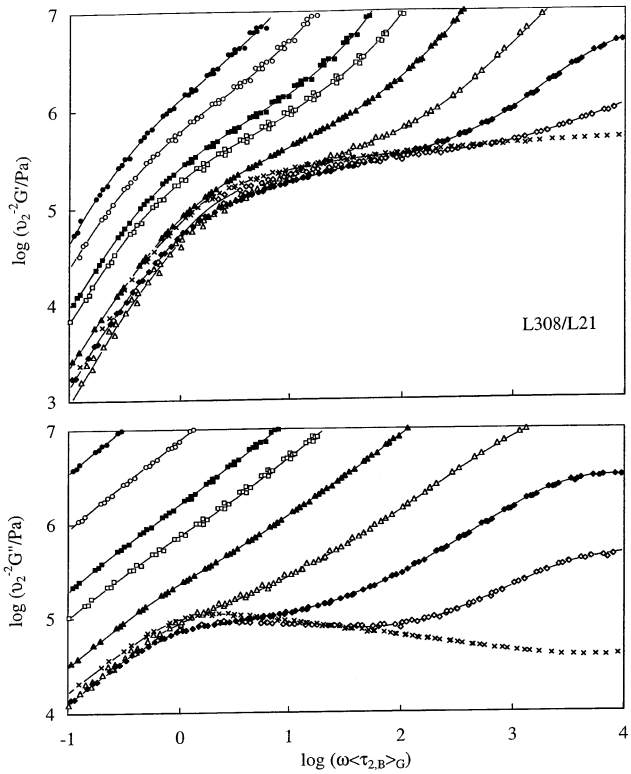

Figure 10. Plots of reduced moduli $\upsilon_2^{-2}G'$ and $\upsilon_2^{-2}G''$ of the L308/L21 blends against the normalized frequency $\omega\langle\tau_{2,B}\rangle_G$. The symbols are the same as in Figure 8.

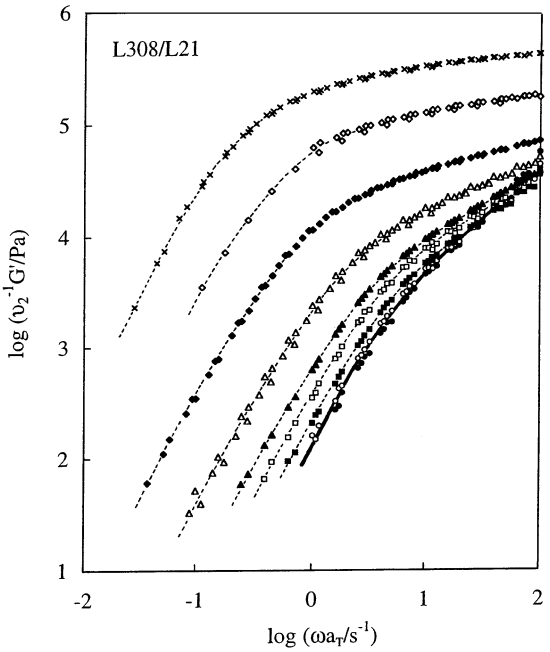

Figure 11. Plots of $\upsilon_2^{-1}G'$ of the L308/L21 blends against the nonnormalized frequency ω. The plots are shown at low ω where the low-M chain (L21) negligibly contributes to G' of the blends. The symbols are the same as in Figure 8.

1.3. Although the reduced plots for $d = 1.2$ were not significantly scattered compared to those in Figures 8 and 9, we choose $d = 1.3$ for definiteness in our later analysis of the DTD picture.

For $\upsilon_2 \leq 0.05$, the reduced plots do not exhibit the universal superposition even for $d = 1.3$; see Figures 8 and 9. This result indicates that the entanglement between the high-M chains is not well developed for $\upsilon_2 \leq 0.05$ and the relaxation mechanism gradually changes with υ_2. This range of υ_2 coincides with a range of $\upsilon_2 < \upsilon_{2,c}$, where $\upsilon_{2,c}$ is the crossover threshold between the dilute and concentrated regimes (cf. eq 7).

For examination of the other type of universality for small υ_2, we focused on G' at low ω that is hardly contributed from the fast relaxation of the low-M chain (the majority component at small υ_2). Figure 11 shows plots of $\upsilon_2^{-1}G'$ against the nonnormalized frequency ω. For very small $\upsilon_2 \leq 0.01$, the plots are collapsed onto a universal curve. This universality, noted also for PS/PS blends,[1] corresponds to the CR relaxation associated with the υ_2-independent $\tau_{CR,G}°$ (cf. Figure 7).

Here, we should make a comment for similarity/difference between the PI/PI (L308/L21) blends and the previously examined PS/PS blends having $r_{GS} > 0.5$. The power-law type υ_2 dependencies ($J_{2,B} \propto \upsilon_2^{-1}$, $\eta_{2,B} \propto \upsilon_2$ for $\upsilon_2 \to 0$ and $J_{2,B} \propto \upsilon_2^{-\alpha}$, $\eta_{2,B} \propto \upsilon_2^{\alpha'}$ for sufficiently large υ_2) were confirmed for those PS/PS blends[1,27,29,36] but their exponents α ($\cong$2) and α' ($\cong$3.5) were somewhat different from those for the PI/PI blends ($\alpha = 2.2-2.3$ and $\alpha' = 3.6-3.7$; cf. eq 6). Furthermore, for the PS/PS blends, the dilation exponent $d = 1$ gave the universal superposition in the reduced plots similar to that in Figure 8; see Figure 27 in ref 1. We reexamined the data of the PS/PS blends and found that the superposition is considerably worse for $d = 1.3$ and the exponent $\alpha = 2.2-2.3$ does not accurately describe the $J_{2,B}$ data for large υ_2. Thus, the d and α values (as well as the α' value) may be moderately different for different polymer species, although more data need to be accumulated for concluding this difference.

3.4. Dielectric Relaxation Times of High-*M* and Low-*M* Chains.

The phenomenological framework of the linear response theory is the same for the viscoelastic and

dielectric relaxation, and the dielectric loss $\epsilon''(\omega)$ and a decrease of the dynamic dielectric constant $\Delta\epsilon'(\omega) = \epsilon'(0) - \epsilon'(\omega)$ are analogous to G'' and G'.[12,14,15] Thus, the dielectric relaxation time of the high-M chain in the blends is evaluated from the data of $\epsilon''(\omega)$ (Figure 4) and $\Delta\epsilon'(\omega)$ (not shown) through a relationship analogous to eq 4,

$$\langle\tau_{2,B}\rangle_\epsilon = \frac{\left[\frac{1}{\omega^2}\{\Delta\epsilon_B'(\omega) - (1 - v_2)\Delta\epsilon_{1,m}'(\omega)\}\right]_{\omega\to 0}}{\left[\frac{1}{\omega}\{\epsilon_B''(\omega) - (1 - v_2)\epsilon_{1,m}''(\omega)\}\right]_{\omega\to 0}} \quad (9)$$

Here, the subscripts 'B' and '1,m' denote the data obtained for the blend and monodisperse system of the low-M chain. This $\langle\tau_{2,B}\rangle_\epsilon$ is close to the longest dielectric relaxation time.[1,15]

For large v_2 where the relaxation of the low-M chain is retarded by the high-M chains, the $\epsilon_{1,m}''(\omega)$ and $\Delta\epsilon_{1,m}'(\omega)$ terms in eq 9 are to be replaced by $\epsilon_{1,m}''(\lambda\omega)$ and $\Delta\epsilon_{1,m}'(\lambda\omega)$ with λ being the retardation factor. However, at low ω, the subtraction in eq 9 is just a minor correction for our blends at large v_2, as similar to the situation explained for eqs 2−4. Thus, eq 9 was utilized in the entire range of v_2 to evaluate $\langle\tau_{2,B}\rangle_\epsilon$. The dielectric relaxation time in the solutions, $\langle\tau_{2,sol}\rangle_\epsilon$, was similarly evaluated from the data for the solutions and pure solvent (B2).

These $\langle\tau_{2,B}\rangle_\epsilon$ and $\langle\tau_{2,sol}\rangle_\epsilon$ excellently agreed with a relaxation time $1/\omega_{p,low}$ evaluated from the angular frequency $\omega_{p,low}$ of the low-ω ϵ'' peak for the high-M chain. This agreement results from a narrow distribution of the terminal dielectric modes reflected in the sharp ϵ'' peak immediately followed by the terminal tail ($\epsilon'' \propto \omega$) at the lower ω side. As noted for the high-ω ϵ'' peak in Figure 4, the low-M chain in the blends has a similarly narrow distribution of its dielectric modes. We utilized the angular frequency $\omega_{p,high}$ of this peak to evaluate the dielectric relaxation time of this chain as $\langle\tau_{1,B}\rangle_\epsilon = 1/\omega_{p,high}$.

In Figure 7, the dielectric relaxation times thus evaluated are shown with the filled symbols. The dielectric $\langle\tau_2\rangle_\epsilon$ and viscoelastic $\langle\tau_2\rangle_G$ of the high-M chain are close to each other in both blends and solutions, confirming again that the viscoelastically detected global motion of the high-M PI chain (L308) is dielectrically active. At the same time, we should note that $\langle\tau_2\rangle_G$ and $\langle\tau_2\rangle_\epsilon$ are not exactly the same. The chain should have $\langle\tau_2\rangle_G = \langle\tau_2\rangle_\epsilon$ if the surrounding tube is fixed in space.[1,11,15] Thus, the small but nonnegligible difference observed for $\langle\tau_2\rangle_G$ and $\langle\tau_2\rangle_\epsilon$ reflects the tube motion.

Now, we turn our attention to the dielectric $\langle\tau_{1,B}\rangle_\epsilon$ of the low-M chain (L21). In a range of $v_2 \le 0.1$, $\langle\tau_{1,B}\rangle_\epsilon$ in the blends (filled triangles in Figure 7) coincides with that in the monodisperse system (horizontal dashed line) and the high-M chains negligibly enhance the entanglement lifetime for the low-M chain. With increasing $v_2 > 0.1$, the high-M chains become sufficiently concentrated to give this enhancement and retard the motion of the low-M chain. The resulting increase of $\langle\tau_{1,B}\rangle_\epsilon$ is utilized in our later analysis of the DTD picture.

4. Discussion

In the remaining part of the paper, we compare the viscoelastic and dielectric data to test the validity of the DTD picture. This test is based on the DTD relationship between the normalized viscoelastic relaxation function of the blend, $\mu(t)$ (=1 at $t = 0$), and the dielectric relaxation functions of the low-M and high-M chains, $\Phi_1(t)$ and $\Phi_2(t)$ both normalized to unity at $t = 0$. This relationship is explained below, and then the test is made for the L308/L21 blends as well as the L308/B2 solutions and monodisperse PI systems.

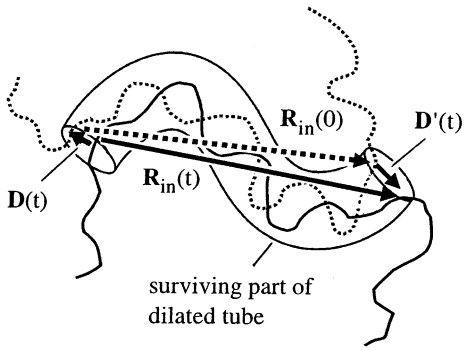

Figure 12. Schematic illustration of the chain in the blend (either the low-M or high-M chain) during the DTD process. Solid and dotted curves indicate the chain at the times t and 0, respectively.

4.1. DTD Relationship.

4.1.1. Formulation. We consider the blend of the low-M and high-M chains (hereafter indexed with $j = 1$ and 2) having the volume fractions v_1 and v_2. In Figure 12, the dotted and solid curves schematically show a chain (either the low-M or high-M chain) in the blend at times 0 and t, respectively. At the time t, the dilated tube partly survives to constrain $N_j\varphi_j'(t)$ entanglement segments of the chain, where N_j is the total number of the segments per chain and $\varphi_j'(t)$ is the survival fraction of the dilated tube for this chain. The average survival fraction $\varphi'(t)$ is given by[1,5]

$$\varphi'(t) = v_1\varphi_1'(t) + v_2\varphi_2'(t) \quad (10)$$

In the DTD picture, the relaxed portion of the high-M and low-M chains is regarded as a solvent.[1,2,5−10] Then, the dilated tube diameter $a'(t)$ is expressed in terms of the average tube survival fraction as $a'(t) = a\{\varphi'(t)\}^{-d/2}$, where a is the diameter of the nondilated tube and d ($\cong$1.3 for PI; cf. Figure 8) is the dilation exponent. The total number of the dilated segments is smaller than that of the entanglement segments by a factor of $\{a/a'(t)\}$,[2] and the stress is sustained by the faction $\varphi'(t)$ of the dilated segments. Thus, $\mu_{DTD}(t)$ of the blend during the DTD process is written as[1,2,5]

$$\mu_{DTD}(t) = \{a/a'(t)\}^2\varphi'(t) = \{\varphi'(t)\}^{1+d} \quad (11)$$

The normalized dielectric relaxation function of the blend as a whole, $\Phi(t)$, is given by

$$\Phi(t) = v_1\Phi_1(t) + v_2\Phi_2(t) \quad (12)$$

The $\Phi_j(t)$ of the component chain ($j = 1$, 2) having the type-A dipoles is given by the autocorrelation of the end-to-end vector $\mathbf{R}_j$,[1,11,15] $\langle\mathbf{R}_j(t)\cdot\mathbf{R}_j(0)\rangle/N_ja^2$ ($\langle\mathbf{R}_j^2\rangle = N_ja^2$ for the Gaussian chain). This correlation is contributed only from a portion of the chain constrained in the surviving part of the dilated tube. Namely, $\Phi_j(t) = \langle\mathbf{R}_{in}(t)\cdot\mathbf{R}_{in}(0)\rangle/N_ja^2$ with $\mathbf{R}_{in}(t)$ and $\mathbf{R}_{in}(0)$ being the end-to-end vector of this portion at the times t and 0;[11] see Figure 12. The chain fluctuates in the two edges of the surviving part of the dilated tube, and $\mathbf{R}_{in}(t)$ is equal to $\mathbf{R}_{in}(0) + \mathbf{D}(t) + \mathbf{D}'(t)$ with $\mathbf{D}(t)$ and $\mathbf{D}'(t)$ being the displacements in

the tube edges due to this fluctuation; cf. Figure 12. Thus, we have $\Phi_j(t) = [\langle\{\mathbf{R}_{in}(0)\}^2\rangle + \langle\mathbf{D}(t)\cdot\mathbf{R}_{in}(0)\rangle + \langle\mathbf{D}'(t)\cdot\mathbf{R}_{in}(0)\rangle]/N_j a^2$. Since the chain at the time 0 has $N_j\varphi_j'(t)$ entanglement segments in this surviving part, we find $\langle\{\mathbf{R}_{in}(0)\}^2\rangle = N_j\varphi_j'(t)a^2$. Furthermore, the Gaussian feature of the chain gives a relatioship,[14,16] $\langle\mathbf{D}(t)\cdot\mathbf{R}_{in}(0)\rangle = \langle\mathbf{D}'(t)\cdot\mathbf{R}_{in}(0)\rangle = -\langle\{\mathbf{D}(t)\}^2\rangle/2$ (for the maximum tube-edge fluctuation effect). This $\langle\{\mathbf{D}(t)\}^2\rangle$ can be evaluated as a mean-square distance of two entanglement segments *randomly located* in the circular edge of the dilated tube,[14,16,37]

$$\langle\{\mathbf{D}(t)\}^2\rangle = \frac{16}{\pi^2\{a'(t) - a\}^4}\int(\mathbf{r} - \mathbf{r}')^2\, d^2\mathbf{r}\, d^2\mathbf{r}' = \left(\frac{a'(t) - a}{2}\right)^2 \quad (13)$$

Here, $\mathbf{r}$ and $\mathbf{r}'$ are the positions of the centers of the two segments, and the integral is conducted in a circular area of the diameter $a' - a$ (the area available for the segment centers). Thus, we obtain[16]

$$\Phi_j(t) = \varphi_j'(t) - \frac{1}{4N_j}[\{\varphi'(t)\}^{-d/2} - 1]^2 \quad (14)$$

(We have utilized the relationship $a'(t) = a\{\varphi'(t)\}^{-d/2}$ in eq 13 to obtain eq 14.)

The DTD relationship between $\mu(t)$ and $\Phi_j(t)$ ($j = 1$, 2), specified by eqs 10, 11, and 14, enables us to test the DTD picture through comparison of the viscoelastic and dielectric data. However, this relationship is to be utilized in a proper way, as explained below.

4.1.2. Usage of DTD Relationship. The dielectric relaxation functions $\Phi_j(t)$ in the entire range of t are unequivocally obtained from analysis of the ϵ'' data. However, the concept of the dilated tube has a sound meaning only in a range of t where the dilated diameter $a'(t)$ ($=a\{\varphi'(t)\}^{-d/2}$) is smaller than the size of the chain $\langle R_j^2\rangle^{1/2} = aN_j^{1/2}$, and eq 14 converting $\Phi_j(t)$ to $\varphi_j'(t)$ is to be utilized only in this limited range of t. We were able to successfully evaluate $\varphi_j'(t)$ from the dielectric data under this limitation. Details of this evaluation are explained in the Appendix, and a brief summary is given below.

For the high-M chain, the above limitation still allowed us to utilize eq 14 in a range of $t \leq 1.5\langle\tau_{2,B}\rangle_\epsilon$ where the whole relaxation process of the blend was observed. Thus, $\varphi_2'(t)$ of this chain at $t \leq 1.5\langle\tau_{2,B}\rangle_\epsilon$ was evaluated from the dielectric data (by numerically solving eq 14). The full relaxation behavior of $\varphi_2'(t)$ in the entire range of t (even beyond $1.5\langle\tau_{2,B}\rangle_\epsilon$) was described by a fitting function determined in the available range of $t \leq 1.5\langle\tau_{2,B}\rangle_\epsilon$.

For the low-M chain, eq 14 was usable only at $t \leq 2\langle\tau_{1,B}\rangle_\epsilon$, i.e., only at $t \ll \langle\tau_{2,B}\rangle_\epsilon$. However, the terminal relaxation of the low-M chain was clearly observed in this range of t, and a fitting function for the $\varphi_1'(t)$ data obtained in that range could successfully describe the full relaxation behavior of $\varphi_1'(t)$. Thus, the limitation in the use of eq 14 did not disturb the calculation of $\mu_{DTD}(t)$ (eqs 10 and 11).

4.2. Test of DTD Picture for Blends.

4.2.1. Test for *G and μ.** For the L308/L21 blend with $v_2 = 0.2$, $G_{DTD}'(\omega)$ and $G_{DTD}''(\omega)$ for the DTD process were calculated as the Fourier transformation of $\mu_{DTD}(t)$ determined with the method explained in the Appendix. In Figure 13, the calculated moduli are compared with the G' and G'' data. For the dilation exponent $d = 1.3$ (determined from the superposition in Figure 8), the moduli calculated in the presence of the tube-edge fluctuation effect (solid curve) agree with the data at low ω but the moduli calculated without this effect (dash−dot curve) significantly deviate from the data. This result demonstrates that the DTD picture is valid for the blend at low ω and that the tube-edge fluctuation has an important effect for the actual DTD process characterized with the exponent $d = 1.3$.

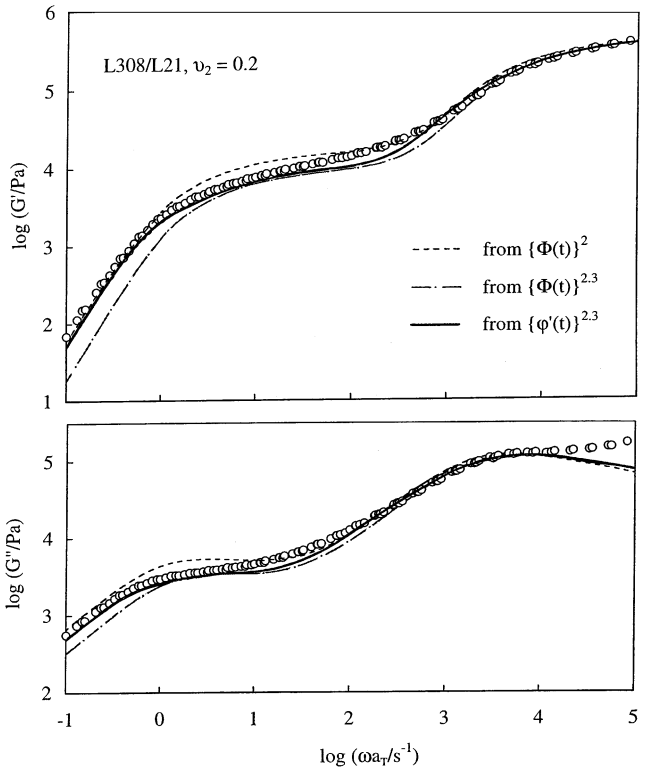

Figure 13. Comparison of the G' and G'' data of the L308/L21 blend ($v_2 = 0.2$; circles) with G_{DTD}' and G_{DTD}'' for the DTD process calculated from the dielectric data. Solid curves indicate G_{DTD}' and G_{DTD}'' calculated for the dilation exponent $d = 1.3$ in the presence of the tube-edge fluctuation effect. Dash−dot and dashed curves, respectively, show the moduli calculated for $d = 1.3$ and $d = 1$, both in the absence of this effect.

In Figure 13, the dashed curves indicate the moduli calculated for the DTD process with $d = 1$ in the absence of the tube-edge fluctuation effect ($\mu_{DTD}(t) = \{\Phi(t)\}^2$). The calculated G_{DTD}' is considerably larger than the G' data at ω/s$^{-1} = 10^0$−10^2 where the high-M chains exhibits the plateau due to their mutual entanglements. This result, naturally expected from the failure of the superposition of $v_2^{-2}G^*$ in Figure 10, again demonstrates that the dilation exponent d for PI chains is larger than 1 and close to 1.3 (although a little smaller exponent of $d = 1.2$ is still acceptable).

The high-M chains are mutually entangled in the blends with $v_2 \geq 0.05$ ($\cong$characteristic $v_{2,c}$ for this entanglement; cf. eq 7). For these blends, we compared the $\mu_{DTD}(t) = \{\varphi'(t)\}^{2.3}$ for the DTD process (for $d = 1.3$ and with the tube-edge fluctuation effect) and the $\mu(t)$ data, the latter being obtained from the G' and G'' data (Figure 2) with an iteration method.[14] The results are summarized in Figure 14. The μ_{DTD} (solid curves) and μ data (symbols) are in good agreement and the DTD picture is valid in short time scales for the terminal relaxation of the low-M chains as well as in long time

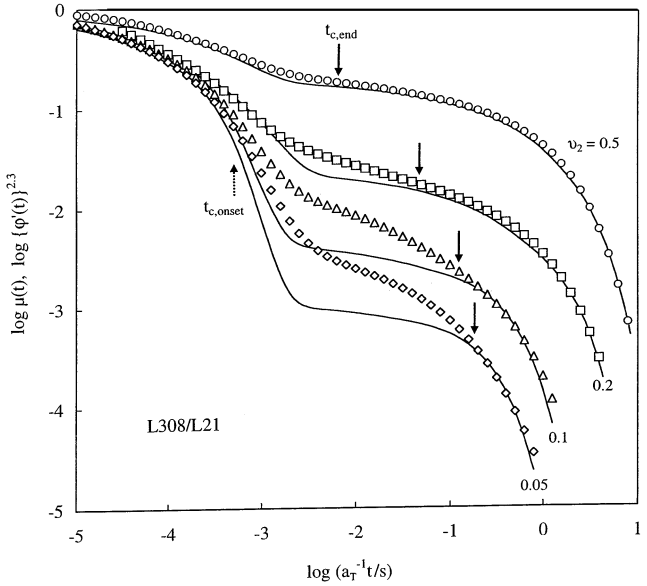

Figure 14. Comparison of $\mu(t)$ data of the L308/L21 blends ($\upsilon_2 \geq 0.05$; symbols) with $\mu_{DTD}(t) = \{\varphi'(t)\}^{2.3}$ calculated for the DTD process with $d = 1.3$ in the presence of the tube-edge fluctuation effect (solid curves). The dotted and solid arrows indicate two characteristic times $t_{c,onset}$ and $t_{c,end}$ for the onset and end of the failure of the DTD picture.

scales for the terminal relaxation of the high-M chain. However, in intermediate time scales, the calculated μ_{DTD} is smaller than the μ data. In Figure 13, the corresponding difference is noted for the G^* data and calculated G_{DTD}^* (solid curves for $d = 1.3$) at intermediate ω. The deviation between the data and DTD calculation, indicating a failure of the DTD picture at intermediate t, is larger for smaller υ_2; see Figure 14.

This failure of the DTD picture is intimately related to a rate of the CR equilibration. The DTD picture assumes that the entanglements between the low-M and high-M chains become ineffective and the CR equilibration of the high-M chains occurs over a distance $a' = \upsilon_2^{-d/2}a$ *immediately after* the low-M chain relaxes. This assumption is reflected in the DTD expression $\mu_{DTD} = \{\upsilon_1\varphi_1'(t) + \upsilon_2\varphi_2'(t)\}^{1+d}$ (eqs 10 and 11) that gives $\mu_{DTD} \cong \{\upsilon_2\varphi_2'\}^{1+d} \cong \upsilon_2^{1+d}$ in a range of $\langle\tau_{1,B}\rangle_\epsilon < t \ll \langle\tau_{2,B}\rangle_\epsilon$ where the low-M chain has fully relaxed ($\varphi_1' \ll 1$) while the high-M chain has hardly escaped from its dilated tube ($\varphi_2' \cong 1$).

However, in the real systems, the CR equilibration of the high-M chain requires a certain time τ^{**} and the DTD picture assuming the instantaneous CR equilibration is valid only at $t > \tau^{**}$. In other words, the entanglement effect of the low-M chain on the motion/relaxation of the high-M chain still remains (by $t \cong \tau^{**}$) after the low-M chain relaxes. This τ^{**} increases with an increase of the number $\beta = \{a'/a\}^2$ of the entanglement segments to be involved in the CR equilibration ($\tau^{**} \propto \beta^2$ for large β),[1] and β increases with t. For this reason, the DTD picture begins to fail at short t (not very different from $\langle\tau_{1,B}\rangle_\epsilon$) where β rapidly increases to $\cong\upsilon_2^{-d}$ and the required CR equilibration cannot occur in time, while this picture recovers its validity at long t ($\gg\langle\tau_{1,B}\rangle_\epsilon$) where β has not significantly increased from υ_2^{-d} and the corresponding τ^{**} becomes shorter than the time scale t. This molecular scenario naturally results in the failure of the DTD picture observed at intermediate t (Figure 14). Indeed, a corresponding

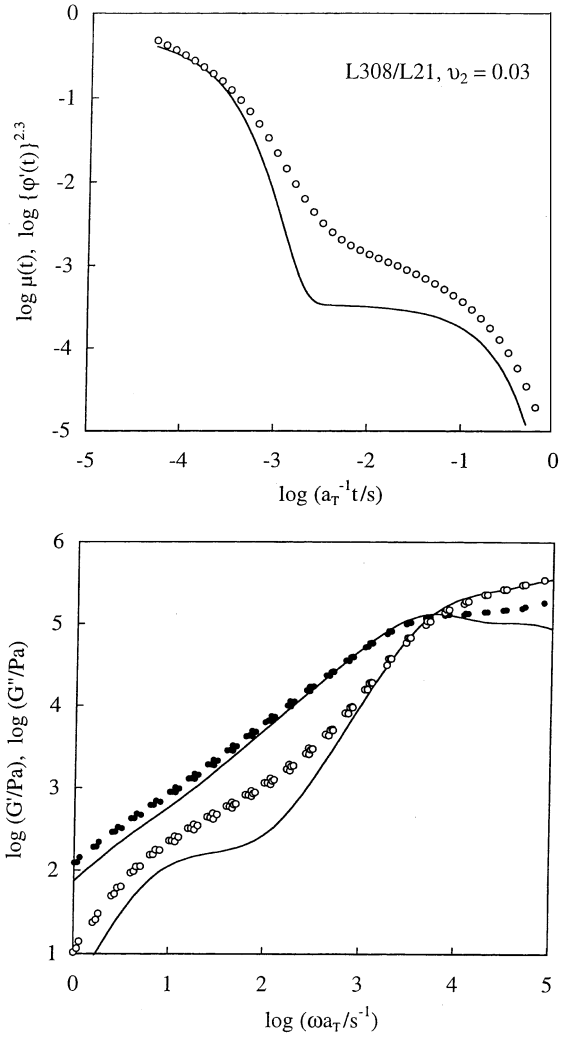

Figure 15. Comparison of μ and G^* data of the L308/L21 blend ($\upsilon_2 = 0.03$; symbols) with those calculated for the DTD process with $d = 1.3$ in the presence of the tube-edge fluctuation effect (solid curves). Note the failure of the DTD picture at long t ($\cong\langle\tau_{2,B}\rangle_G$; top panel) and low ω ($\cong 1/\langle\tau_{2,B}\rangle_G$; bottom panel).

failure has been noted for blends of star and linear chains[10] (although the failure was concluded from comparison of the tube model and viscoelastic data, not from the comparison of the viscoelastic and dielectric data made in this study). This failure of the DTD picture for our linear/linear blends is further examined later in relation to two characteristic times for the onset and end of the failure.

4.2.2. Additional Comment. Here, a comment needs to be made for the difference between the calculated μ_{DTD} and measured μ at intermediate t. The above molecular scenario suggests that a decrease of υ_2 leads to an increase of the β value at $t \cong \langle\tau_{1,B}\rangle_\epsilon$, thereby enhancing this difference. Equivalently, the difference between μ_{DTD} and μ becomes undetectably small with increasing υ_2 (above 0.5 for our L308/L21 blends; see Figure 14). Thus, experiments in a wide range of υ_2 is essential for the tests of the DTD picture and a related molecular picture of double reptation.[38]

We should also emphasize that the DTD picture fails even at long $t \cong \langle\tau_{2,B}\rangle_\epsilon$ for dilute high-M chains entangled only with the low-M chains. An example is shown in Figure 15 for the blend with $\upsilon_2 = 0.03$ ($<\upsilon_{2,c}$). The difference between the data (symbols) and DTD calcula-

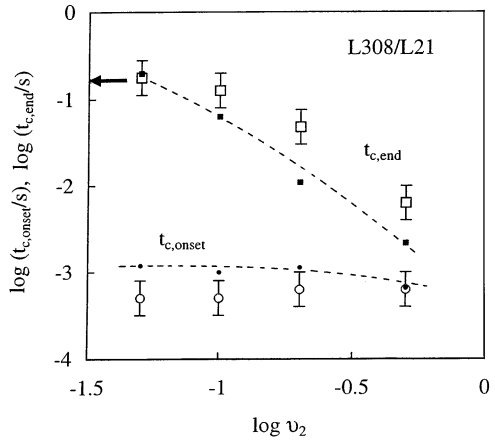

Figure 16. Characteristic times $t_{c,onset}$ and $t_{c,end}$ for the onset and end of the failure of the DTD picture for the L308/L21 blends with $\upsilon_2 \geq 0.05$ (large unfilled symbols). Small filled symbols show these times evaluated from the Rouse CR model (cf. eq 15). The horizontal arrow indicates the dielectric CR relaxation time for the *dilute* high-M chain. For further details, see text.

tion (solid curves) at long t/low ω is mainly due to a difference in the terminal viscoelastic relaxation intensity: The intensity deduced from the DTD picture scales as υ_2^{1+d} (cf. eqs 10 and 11), while the observed intensity ($\sim 1/J_{2,B}$; Figure 6) scales as υ_2 in the dilute regime. In the dilute limit ($\upsilon_2 \rightarrow$ f 0) where this DTD intensity factor υ_2^{1+d} vanishes, the DTD picture predicts that the high-M chain fully relaxes at $t \cong \langle\tau_{1,B}\rangle_\epsilon$ together with the low-M chain.[11] Obviously, this prediction completely fails: The very dilute high-M chain fully relaxes through the CR mechanism at $t \gg \langle\tau_{1,B}\rangle_\epsilon$, as noted in Figure 2.

4.2.3. Onset and End of the Failure of DTD Picture. For the concentrated blends with $\upsilon_2 \geq 0.05$, the DTD picture fails at intermediate t; see Figure 14. We evaluated two characteristic times $t_{c,onset}$ and $t_{c,end}$ for the onset and end of this failure as the times where the calculated μ_{DTD} curve began to deviate from and merge into the μ data. These $t_{c,onset}$ and $t_{c,end}$ (dotted and solid arrows in Figure 14) were determined with acceptable uncertainties (about ±50%).

Figure 16 shows dependence of these $t_{c,onset}$ and $t_{c,end}$ on υ_2. The horizontal arrow indicates the dielectric CR relaxation time for the dilute high-M chain, $\tau_{CR,\epsilon}°$ (eq 8). The $t_{c,onset}$ hardly changes with υ_2, while $t_{c,end}$ decreases from this $\tau_{CR,\epsilon}°$ with increasing υ_2. Although the $t_{c,onset}$ and $t_{c,end}$ values include the above uncertainty (shown with the error bar in Figure 16), these qualitative features of $t_{c,onset}$ and $t_{c,end}$ are clearly noted in Figure 14. Thus, the DTD picture fails in a wider range of t for smaller υ_2.

Here, we attempt to evaluate the CR equilibration time τ^{**} on the basis of the Rouse-like CR model[1,3] for the high-M chain composed of N_2 entanglement segments ($N_2 \cong 62$). For the tube to dilate to a diameter $a' = \beta^{1/2}a$, the CR equilibration needs to occur over successive β entanglement segments of this chain. Since this equilibration corresponds to N_2/β-th Rouse-CR mode, its characteristic time can be expressed as[1,3,39]

$$\tau^{**}(\beta) = \tau_{CR,\epsilon} \sin^2\left(\frac{\pi}{2N_2}\right) \sin^{-2}\left(\frac{\pi}{2\beta}\right) \qquad (15)$$

Here, $\tau_{CR,\epsilon}$ is the characteristic time of the slowest Rouse CR mode, i.e., the time required for the CR equilibration over the whole contour of the chain. (For $\beta > 3$, eq 15 is numerically very close to the familiar relationship,[1] $\tau^{**} = \tau_{CR,\epsilon}\{\beta/N_2\}^2 \propto \beta^2$.)

This $\tau_{CR,\epsilon}$ is equivalent to $\tau_{CR,\epsilon}°$ for the dilute high-M chain *except* that the motion of the low-M chain activating the CR equilibration is slower in the concentrated blend (with large υ_2) than in the dilute blend (with $\upsilon_2 \rightarrow 0$) and that the number density ν_{h-1} of the entanglement between the low-M and high-M chains is smaller in the concentrated blend by a factor of $1 - \upsilon_2$. Thus, we may estimate $\tau_{CR,\epsilon}$ as

$$\tau_{CR,\epsilon} = \tau_{CR,\epsilon}° f_r \frac{1}{1-\upsilon_2} \quad \text{with } f_r = \frac{\langle\tau_{1,B}\rangle_\epsilon}{\langle\tau_{1,m}\rangle_\epsilon} \qquad (16)$$

Here, $\langle\tau_{1,m}\rangle_\epsilon$ and $\langle\tau_{1,B}\rangle_\epsilon$ are the dielectric relaxation time of the low-M chain in its monodisperse system and in the concentrated blend, respectively, and their ratio, f_r, gives a correction for the above difference in the low-M chain motion. The $1/(1 - \upsilon_2)$ factor accounts for a decrease of the local CR jump frequency (∝ number of CR-jump sites) due to the decrease of ν_{h-1}.

For the blends examined in Figure 16, the parameters appearing in eqs 15 and 16 can be determined from data: $\tau_{CR,\epsilon}°$ is given in eq 8, f_r is obtained from the $\langle\tau_{1,B}\rangle_\epsilon$ data shown in Figure 7, and β for the DTD process at respective t is evaluated from the $\{\varphi'(t)\}^{2.3}$ curves shown in Figure 14; $\beta(t) = \{\varphi'(t)\}^{-d}$ with $d = 1.3$. Thus, we evaluated the times τ_{onset}^{**} and τ_{end}^{**} required for the CR equilibration in those blends at $t_{c,onset}$ and $t_{c,end}$, respectively. These τ^{**} are shown in Figure 16 with the small filled symbols connected with the dotted curves. The τ_{onset}^{**} agrees well with $t_{c,onset}$, and τ_{end}^{**} is close to $t_{c,end}$ (as judged from the uncertainty in the $t_{c,end}$ value). This result strongly suggests that the DTD picture begins to fail at $t \cong t_{c,onset}$ (where τ^{**} becomes larger than t) and becomes valid again at $t \cong t_{c,end}$ (where τ^{**} becomes smaller than t), lending support to our molecular scenario.

4.3. Comparison of Blends and Solutions. The above test of the DTD picture examined the validity of the DTD relationship for the viscoelastic and dielectric data of the L308/L21 blends. In other words, this picture may hold even if the slow viscoelastic mode distribution of the high-M chain in the blends *does not* coincide with that in the L308/B2 solution. For a test of this coincidence, we utilized eq 2 to subtract the contribution of the low-M chain (L21) and/or the solvent (B2) from the G' data of the blends/solutions and evaluate the storage modulus G_2' of the high-M chains therein. At low ω, G_2' is insensitive to the fast modes of the high-M chain (due to its motion within the entanglement segment). Thus, a comparison of G_2' for the blends and solutions allows us to most clearly test the coincidence of the slow mode distribution in these systems. (The loss modulus G_2'' of the high-M chain, being rather sensitive to the fast modes, was not utilized in this test.)

Figure 17 compares G_2' for the blends (circles) and the solutions (solid curves). The comparison is made at low ω where the above subtraction gave only minor corrections for the raw G' data. For clear comparison of the slow viscoelastic mode distribution in the blends and solutions, the G_2' curves for the solutions are shifted along the ω axis so that their terminal tails are superposed on the tails of G_2' for the blends.

In Figure 17, the dotted arrows show the characteristic frequency $1/t_{c,end}$ for the end of the failure of the DTD picture (cf. Figures 14 and 16), and the solid

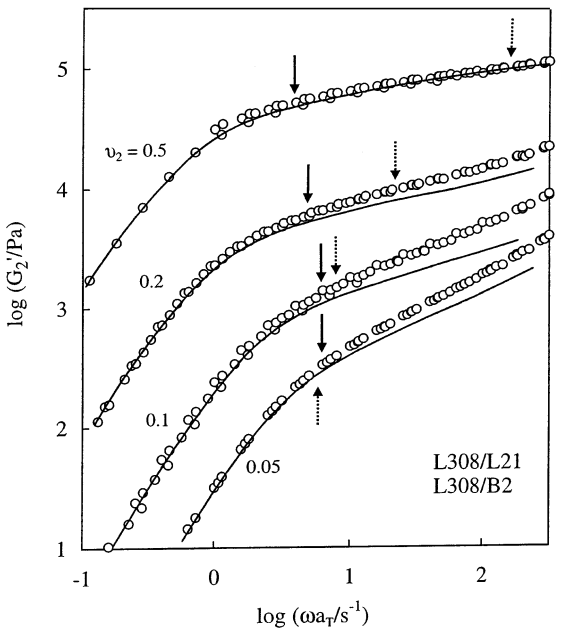

Figure 17. Comparison of G_2' of the high-M chain (L308) in the L308/L21 blends (circles) and the L308/B2 solutions (solid curves). For clear comparison of the slow viscoelastic mode distribution reflected in the ω dependence of G_2', the G_2' curves for the solutions are shifted along the ω axis so that their terminal tails are superposed on the tails of G_2' for the blends. The dotted arrows show the characteristic frequency $1/t_{c,end}$ for the end of the failure of the DTD picture in the blends, and the solid arrows indicate the frequency $1/\tau_{CR,\epsilon}$ for the CR equilibration over the whole contour of the high-M chain (cf. eq 16).

arrows indicate the frequency $1/\tau_{CR,\epsilon}$ for the CR equilibration over the whole contour of the high-M chain (cf. eq 16). For $\upsilon_2 = 0.2$, G_2' for the blend begins to deviate from G_2' for the solution as ω is increased above $1/\tau_{CR,\epsilon}$, and a considerably large deviation is noted at $\omega = 1/t_{c,end}$. Thus, the blend and solution exhibit the same viscoelastic mode distribution only at $\omega < 1/\tau_{CR,\epsilon}$ or, equivalently, only at $t > \tau_{CR,\epsilon}$.

For the blends/solutions with $\upsilon_2 = 0.1$ and 0.05, the frequencies $1/\tau_{CR,\epsilon}$ and $1/t_{c,end}$ are close to each other and the deviation of G_2' at $\omega = 1/t_{c,end}$ is not clearly distinguished from the onset of deviation at $\omega = 1/\tau_{CR,\epsilon}$. However, the G_2' data shown in Figure 17 still allow us to conclude that the deviation occurs at $\omega > 1/\tau_{CR,\epsilon}$ also for those blends and solutions.

For the blend and solution with large υ_2 (=0.5), the deviation of G_2' is small in the entire range of ω examined because the slow dynamics in these systems is commonly dominated by the dense entanglements between the high-M chains therein. However, this result does not rule out a conclusion that a minor deviation occurs at $\omega > 1/\tau_{CR,\epsilon}$ for $\upsilon_2 = 0.5$.

The above results, in particular those for $\upsilon_2 \leq 0.2$, suggest that the viscoelastic mode distribution of the high-M chain in the blends coincides with that in the solutions only after the CR equilibration occurs over the *whole contour* of the chain. Thus, the high-M chain motion in the blend being free from the entanglement with the low-M chains, i.e., the motion similar to that in the solution, appears to occur only after this equilibration. In other words, the rather local CR equilibration over the dilated tube diameter a' is not sufficient to allow this free motion. These features have been noted also for PS/PS blends.[1]

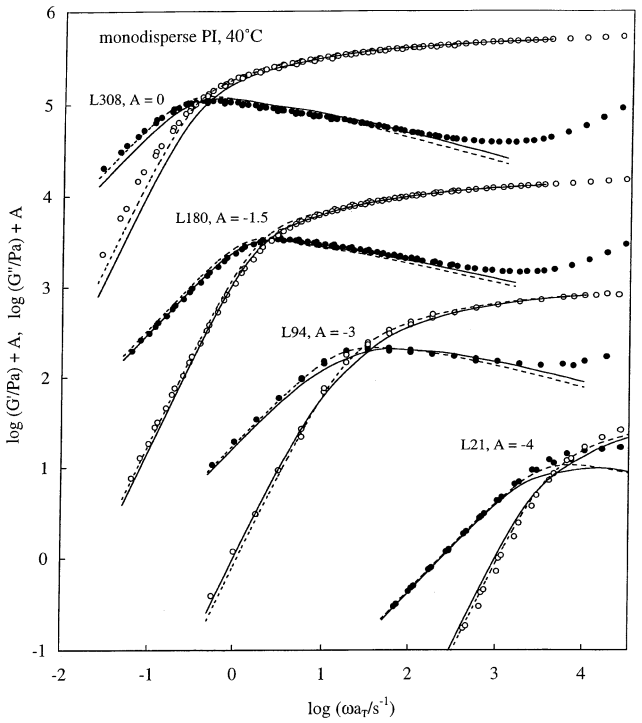

Figure 18. Comparison of G' (unfilled circles) and G'' (filled circles) of monodisperse melt PI with the moduli for the DTD process. The DTD moduli calculated for $d = 1.3$ in the presence of the tube-edge fluctuation effect are shown with the solid curves, and those for $d = 1$ in the absence of this effect are shown with the dotted curves.

4.4. Test of DTD Picture for Monodisperse Melts and Solutions.

For the entangled monodisperse PI melts as well as entangled L308/B2 solutions (with $\upsilon_2 \geq 0.1$), we utilized the ϵ'' data to calculate G_{DTD}' and G_{DTD}'' for the DTD process with the method explained in Appendix (but without the separation of the ϵ'' data). In Figure 18, G_{DTD}' and G_{DTD}'' of the monodisperse melts of various M (Table 1) calculated for $d = 1.3$ in the presence of the dilated tube-edge fluctuation effect are shown with the solid curves, and those for $d = 1$ in the absence of this effect are shown with the dotted curves. For the L308/B2 solutions, G_{DTD}' and G_{DTD}'' for $d = 1.3$ (with the tube-edge effect) and $d = 1$ (without this effect) are shown in Figure 3 with the solid and dotted curves, respectively.

In Figures 3 and 18, we note that the DTD curves for $d = 1.3$ and $d = 1$ are close to each other and well describe the viscoelastic data (symbols) at low ω. Thus, the validity of the DTD picture at long times is confirmed for the monodisperse melts and solutions of linear PI chains.

Here, we have to add a comment for the close coincidence of the DTD curves for $d = 1.3$ and $d = 1$. This coincidence is a natural consequence of a fact that the dilated tube has a considerably large survival fraction $\varphi'(t)$ even at the viscoelastic terminal relaxation time $\langle\tau\rangle_G = J\eta$ because of the narrow distribution of the motional modes of the linear chains; $\varphi'(t) \cong 0.3$ at $t = \langle\tau\rangle_G$: For such large $\varphi'(t)$, the tube-edge effect (of the order of $[\{\varphi'(t)\}^{-d/2} - 1]^2/4N$; cf. eq 14) is minor in the entire range of $t \leq \langle\tau\rangle_G$ and no significant difference is found between $\mu_{DTD} = \{\varphi'(t)\}^{2.3}$ (for $d = 1.3$ and with the tube-edge effect) and $\mu_{DTD} = \{\Phi(t)\}^2$ (for $d = 1$ and without this effect).

For this reason, the simplest DTD picture ($d = 1$ and without tube-edge effect) can describe the data for the monodisperse linear PI chains, as noted previously.[11,14−16] However, the results for the blends presented in this paper unequivocally indicate that the dilation exponent d for PI is larger than 1 and close to 1.3 and that the tube-edge fluctuation has an important effect in the dynamic behavior of the blends (having considerably small $\varphi'(t) \cong v_2\varphi_2'(t)$ at long t). Although a question was recently posed on the tube-edge effect,[40] the experimental results presented in this study demonstrate the importance of this effect in the entanglement dynamics.[41]

5. Concluding Remarks.

We have examined viscoelastic and dielectric relaxation behavior of entangled binary blends of linear PI having widely separated molecular weights ($M_1 \cong 4M_e$ and $M_2 \cong 62M_e$) and various volume fractions v_2 of the high-M chain. The Struglinski-Graessley parameter, $M_2M_e^2/M_1^3 = 0.79$, was larger than a threshold value $\cong$0.5 necessary for the thermal constraint release (CR) mechanism to dominate the relaxation of the dilute high-M chain, and the Rouse-like CR relaxation of this chain was indeed detected for $v_2 \leq 0.01$.

For $v_2 \geq 0.05$, the high-M chains were entangled with each other and their terminal relaxation behavior was qualitatively similar to that in solutions (in the nonentangling solvent B2). In this terminal regime, comparison of the viscoelastic and dielectric data suggested the validity of the dynamic tube dilation (DTD) picture for $d \cong 1.3$ incorporating the tube-edge fluctuation effect.

It should be emphasized that the DTD picture without the tube-edge fluctuation effect failed to describe the dynamic behavior of the high-M chains in the blends. This result demonstrates the importance of this effect for the case of significant dilation of the tube (which resulted from the relaxation of the low-M chains in the blends). However, in monodisperse melts/solutions, the tube dilated only moderately and even the simplest DTD picture (for $d = 1$ and without the tube-edge fluctuation effect) was approximately valid.

In intermediate time scales that were still longer than the relaxation time of the low-M chains, the moduli of the high-M chains in the blends were larger than the DTD prediction. In this intermediate regime, the CR equilibration of the entanglement segments in the dilated tube segment (the prerequisite of DTD) could not occur in time, thereby resulting in this failure of the DTD picture (for $d = 1.3$ and with the tube-edge fluctuation effect). In addition, the viscoelastic mode distribution of the high-M chains in the blends ($v_2 \geq 0.05$) agreed with that in the corresponding solutions only in time scales longer than the time required for the CR equilibration over the whole contour of the chain. These results demonstrate the importance of the CR equilibration in the entanglement dynamics.

Appendix. Analysis of ϵ'' Data and Calculation of μ_{DTD}

The ϵ'' data were analyzed for the evaluation of the survival fraction $\varphi_j'(t)$ of the dilated tube ($j = 1$ and 2 for the low-M and high-M chains), and these $\varphi_j'(t)$ were utilized to calculate the normalized viscoelastic relaxation function $\mu_{DTD}(t)$ for the DTD process. The methods of the analysis and calculation are summarized below.

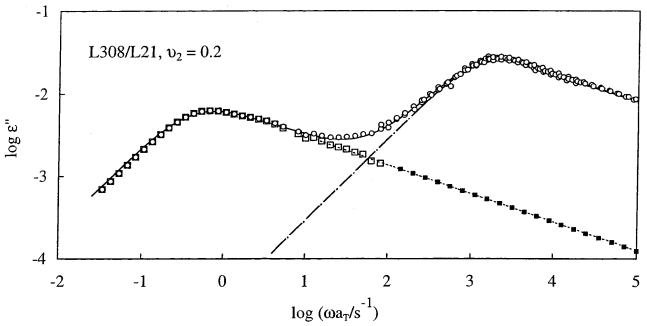

Figure 19. Separation of the ϵ'' data of the L308/L21 blend with $v_2 = 0.2$ (circles) into the contributions $\epsilon_{1,B}''$ (dash−dot curve) and $\epsilon_{2,B}''(\omega)$ (squares) from the low-M and high-M chains in the blend. For details of the separation method, see the Appendix.

A1. DTD in the Presence of Tube-Edge Fluctuation Effect. In the presence of the fluctuation at the dilated tube edge, the dielectric relaxation function $\Phi_j(t)$ is not identical to $\varphi_j'(t)$ and eq 14 (converting Φ_j into φ_j') can be utilized only in a range of t where the dilated tube diameter $a'(t)$ is smaller than the chain size $aN_j^{1/2}$. Under this limitation, we analyzed the ϵ'' data to evaluate $\varphi_j'(t)$ in the following way.

In the analysis, we focused on the fact that the slow dielectric mode distribution of the low-M chain is hardly affected by the high-M chains and insensitive to v_2; see the shape of the high-ω ϵ'' peak in Figure 4. Considering this insensitivity, we utilized the dielectric loss $\epsilon_{1,m}''$ of the monodisperse system of the low-M chain (unfilled circles in Figure 4) to represent the dielectric loss of the low-M chains *in the blend* as $\epsilon_{1,B}''(\omega) = v_1\epsilon_{1,m}''(\omega\lambda)$. Here, v_1 is the volume fraction of the low-M chain in the blend, and λ is a ratio of the high-ω ϵ'' peak frequencies in the blend and monodisperse system. This λ represents the retardation of the motion of the low-M chain due to the high-M chains.

The dielectric loss $\epsilon_{2,B}''(\omega)$ of the high-M chain was obtained by subtracting this $\epsilon_{1,B}''(\omega)$ from the $\epsilon''(\omega)$ data of the blend. As an example, Figure 19 shows the result of this subtraction for $v_2 = 0.2$. At $\omega < 100$ s^{-1}, $\epsilon_{1,B}''$ (dash−dot curve) was sufficiently smaller than the ϵ'' data (circles) to allow an accurate evaluation of $\epsilon_{2,B}''(\omega) = \epsilon''(\omega) - \epsilon_{1,B}''(\omega)$. The $\epsilon_{2,B}''(\omega)$ thus obtained (unfilled squares) exhibited power-law type ω dependence at $\omega = 3-100$ s^{-1}, and $\epsilon_{2,B}''(\omega)$ at higher ω (filled squares) was evaluated by extrapolating this dependence. This extrapolated $\epsilon_{2,B}''(\omega)$ was much smaller than $\epsilon_{1,B}''(\omega)$ at $\omega > 100$ s^{-1} and a sum $\epsilon_{2,B}''(\omega) + \epsilon_{1,B}''(\omega)$ agreed with the $\epsilon''(\omega)$ data at those ω (as well as at lower ω). Thus, the data of the blend with $v_2 = 0.2$ were successfully separated into the contributions $\epsilon_{1,B}''(\omega)$ and $\epsilon_{2,B}''(\omega)$ from the low-M and high-M chains. The separation was equally well achieved for all blends examined.

These $\epsilon_{1,B}''(\omega)$ and $\epsilon_{2,B}''(\omega)$ data were analyzed with a previously reported iteration method[14] to give the dielectric spectra and the corresponding relaxation functions $\Phi_j(t)$ of the low-M and high-M chains ($j = 1$, 2). For these $\Phi_j(t)$, eq 14 was numerically solved to obtain the tube survival fractions $\varphi_j'(t)$. As an example, $\Phi_j(t)$ and $\varphi_j'(t)$ for the blend with $v_2 = 0.2$ are shown in Figure 20. The thick vertical arrows indicate the dielectric relaxation times $\langle\tau_{1,B}\rangle_\epsilon$ and $\langle\tau_{2,B}\rangle_\epsilon$ of the low-M and high-M chains. Note that $\Phi_j(t)$ (squares) relaxes a

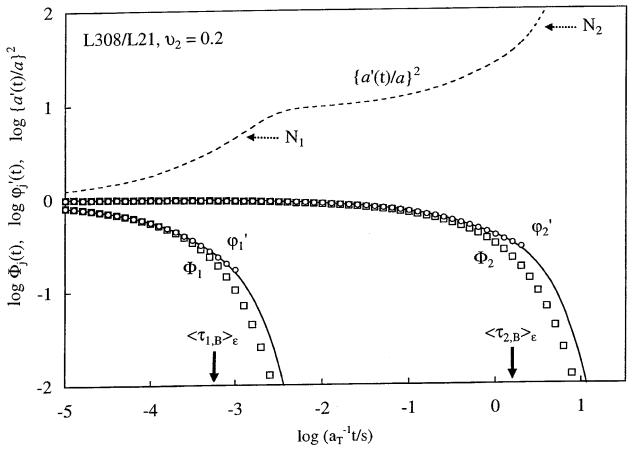

Figure 20. Dielectric relaxation function $\Phi_j(t)$ (squares) and survival fraction of the dilated tube $\varphi_j'(t)$ (circles) for the low-M and high-M chains ($j = 1$ and 2) in the L308/L21 blend with $\upsilon_2 = 0.2$. The $\varphi_j'(t)$ data were obtained from $\Phi_j(t)$ (cf. eq 14) in the ranges of t where $\{a'(t)/a\}^2$ (=$\{\varphi'(t)\}^{-d}$ with $d = 1.3$; dashed curve) is smaller than N_j (horizontal dotted arrows). Solid curves indicate fitting functions $\varphi_{j,fit}'(t) = \Sigma_{p\geq 1} g_{j,p}' \exp(-t/\tau_{j,p}')$ for the $\varphi_j'(t)$ data available in these ranges of t. For further details, see Appendix.

little faster than $\varphi_j'(t)$ (circles) because of the tube-edge fluctuation effect.

Equation 14 can be utilized only when $\{a'(t)/a\}^2$ (= $\{\varphi'(t)\}^{-d}$ with $d = 1.3$; dashed curve) is smaller than N_j (horizontal dotted arrows), and this inequality was satisfied at $t < 2\langle\tau_{1,B}\rangle_\epsilon$ for the low-M chain and at $t < 1.5\langle\tau_{2,B}\rangle_\epsilon$ for the high-M chain; see Figure 20. Thus, $\varphi_j'(t)$ shown in Figure 20 were evaluated only in these limited ranges of t. However, these ranges were still wide enough to cover the terminal relaxation of $\varphi_j'(t)$. Thus, we could utilize fitting functions $\varphi_{j,fit}'(t) = \Sigma_{p\geq 1} g_{j,p}' \exp(-t/\tau_{j,p}')$ (solid curves) to describe the full relaxation behavior of the $\varphi_j'(t)$ data. The same procedure was successfully achieved for all blends examined.

From these $\varphi_{j,fit}'(t)$, the viscoelastic relaxation function for the DTD process in the entire range of t was calculated as $\mu_{DTD}(t) = \{\upsilon_1\varphi_{1,fit}'(t) + \upsilon_2\varphi_{2,fit}'(t)\}^{1+d}$; cf. eqs 10 and 11. (At $t > 2\langle\tau_{1,B}\rangle_\epsilon$ where $\{a'(t)/a\}^2 > N_1$, this $\mu_{DTD}(t)$ was numerically close to the modulus $\{\upsilon_2\varphi_{2,fit}'(t)\}^{1+d}$ without any contribution from the low-M chain.) For the blends with various υ_2 ($\geq$0.1), the $\mu_{DTD}(t)$ for $d = 1.3$ is shown in Figure 14 with the solid curves. The $G_{DTD}'(\omega)$ and $G_{DTD}''(\omega)$ shown in Figure 13 (solid curves) were obtained from Fourier transformation of this $\mu_{DTD}(t)$.

A2. DTD in the Absence of Tube-Edge Fluctuation Effect. In the absence of the tube-edge fluctuation effect, $\varphi_j'(t)$ coincides with $\Phi_j(t)$ obtained from the above analysis of the ϵ'' data; see eq 14 without the second term. Since the terminal relaxation of $\Phi_j(t)$ was observed in the range of t where $\{a'(t)/a\}^2 < N_j$ and eq 14 was usable (cf. Figure 20), the fitting functions $\varphi_{j,fit}'(t)$ (=$\Phi_j(t)$) were utilized to evaluate $\mu_{DTD}(t) = \{\upsilon_1\varphi_{1,fit}'(t) + \upsilon_2\varphi_{2,fit}'(t)\}^{1+d}$ in the entire range of t.

For the blend with $\upsilon_2 = 0.2$, $G_{DTD}'(\omega)$ and $G_{DTD}''(\omega)$ (Fourier transformation of μ_{DTD}) for $d = 1$ and 1.3 are shown in Figure 13 with the dotted and dash−dot curves, respectively.

References and Notes

(1) Watanabe, H. *Prog. Polym. Sci.* **1999**, *24*, 1253−1403.
(2) McLeish, T. C. B. *Adv. Phys.* **2002**, *51*, 1379−1527.
(3) Graessley, W. W. *Adv. Polym. Sci.* **1982**, *47*, 67−117.
(4) Doi M.; Edwards, S. F. *The Theory of Polymer Dynamics*; Clarendon: Oxford, 1986.
(5) Marrucci, G. J. *Polym. Sci. Polym. Phys. Ed.* **1985**, *23*, 159−177.
(6) Ball, R. C.; McLeish, T. C. B. *Macromolecules* **1989**, *22*, 1911−1913.
(7) Milner, S. T.; McLeish, T. C. B. *Macromolecules* **1997**, *30*, 2159−2166.
(8) Milner, S. T.; McLeish, T. C. B. *Macromolecules* **1998**, *31*, 7479−7482.
(9) Colby, R. H.; Rubinstein, M. *Macromolecules* **1990**, *23*, 2753−2756.
(10) Milner, S. T.; McLeish, T. C. B.; Young, R. N.; Hakiki, A.; Johnson, J. M. *Macromolecules* **1998**, *31*, 9345−9353.
(11) Matsumiya, Y.; Watanabe, H.; Osaki K. *Macromolecules* **2000**, *33*, 499−506.
(12) Watanabe, H.; Matsumiya, Y.; Osaki, K. *J. Polym. Sci. Part B: Polym. Phys.* **2000**, *38*, 1024−1036.
(13) Matsumiya, Y.; Watanabe, H. *Macromolecules* **2001**, *34*, 5702−5710.
(14) Watanabe, H.; Matsumiya, Y.; Inoue, T. *Macromolecules* **2002**, *35*, 2339−2357.
(15) Watanabe, H. *Macromol. Rapid Commun.* **2001**, *22*, 127−175.
(16) Watanabe, H. *Korea-Australia Rheol. J.* **2001**, *13*, 205−217.
(17) Watanabe, H.; Sato, T.; Osaki, K. *Macromolecules* **1996**, *29*, 104−112.
(18) Riande, E.; Saiz, E. *Dipole Moments and Birefringence of Polymers*; Prentice Hall: Englewood Cliffs, NJ, 1992.
(19) Nemoto, N.; Moriwaki, M.; Odani, H.; Kurata, M. *Macromolecules* **1971**, *4*, 215−219.
(20) Ferry, J. D. *Viscoelastic Properties of Polymers*, 3rd ed.; Wiley: New York, 1980.
(21) (a) The narrowing of the dielectric mode distribution in the L308/B2 solutions at small υ_2 is attributed to a reduction in the motional cooperativity of the L308 chains, as discussed previously for similar PI solutions.[21b,22c] (b) Watanabe, H.; Yamada, H.; Urakawa, O. *Macromolecules* **1995**, *28*, 6443−6453. (c) Watanabe, H.; Urakawa, O.; Yamada, H.; Yao, M.-L. *Macromolecules* **1996**, *29*, 755−763.
(22) Graessley, W. W. *Adv. Polym. Sci.* **1974**, *16*, 1−179.
(23) Watanabe, H.; Kotaka, T. *Macromolecules* **1984**, *17*, 2316−2325.
(24) Watanabe, H.; Sakamoto, T.; Kotaka, T. *Macromolecules* **1985**, *18*, 1008−1015.
(25) Watanabe, H.; Sakamoto, T.; Kotaka, T. *Macromolecules* **1985**, *18*, 1436−1442.
(26) Watanabe, H.; Kotaka, T. *Macromolecules* **1986**, *19*, 2520−2524.
(27) Watanabe, H.; Kotaka, T. *Nihon Reoroji Gakkaishi (J. Soc. Rheol. Jpn.)* **1987**, *15*, 48−55.
(28) Watanabe, H.; Yamazaki, M.; Kotaka, T. *Macromolecules* **1988**, *21*, 2175−2187.
(29) Watanabe, H.; Yamazaki, M.; Yoshida, H.; Kotaka, T. *Macromolecules* **1991**, *24*, 5573−5581.
(30) Struglinski, M. J.; Graessley, W. W. *Macromolecules* **1985**, *18*, 2630−2643.
(31) The CR-threshold value obtained from a survey of extensive data,[1] $r_{SG} \cong 0.5$, is larger than that reported by Struglinski and Graessley ($r_{SG} \cong 0.1$).[30]
(32) Yoshida, H.; Watanabe, H.; Kotaka, T. *Macromolecules* **1991**, *24*, 572−577.
(33) The $\langle\tau_{2,B}\rangle_G$ defined by eq 4 is related to the relaxation spectrum $H_{2,B}(\tau)$ of the high-M chains in the blends as[1,25] $\langle\tau_{2,B}\rangle_G = [\int_{-\infty}^{\infty} H_{2,B}(\tau)\,\tau^2\,d\ln\tau]/[\int_{-\infty}^{\infty} H_{2,B}(\tau)\,\tau\,d\ln\tau]$. This $\langle\tau_{2,B}\rangle_G$ is an average heavily weighing on slow modes and close to the longest viscoelastic relaxation time.
(34) Colby, R. H.; Rubinstein, M. *Macromolecules* **1990**, *23*, 2753−2756.
(35) Park, S.; Larson, R. G. *J. Rheol.* **2003**, *47*, 199−211.
(36) Watanabe, H.; Kotaka, T. *Macromolecules* **1987**, *20*, 535−543.
(37) The normalization factor in eq 13, $16/\pi^2\{a' - a\}$,[4] was misprinted as $1/\pi^2(a'/2)^4$ in refs 14 and 16.
(38) (a) The test of the double reptation model[38b] was made mostly for blends having large υ_2 (>0.5). For such large υ_2, it is difficult to detect an existing difference between this model and the data, as similar to the situation for the test of the

DTD picture presented in this paper. (b) des Cloizeaux, J. *Macromolecules* **1990**, *23*, 3992−4006.
(39) Although the actual CR process is not perfectly described by the Rouse-CR dynamics (as reveled from analysis of dielectric data for dipole-inverted PI chains), the relaxation time span of the CR eigenmodes is close to that deduced from the Rouse CR dynamics.[1,15] This allows us to utilize eq 15 in the evaluation of τ^{**}.
(40) McLeish, T. C. B. *J. Rheol.* **2003**, *47*, 177−198.
(41) Highly entangled monodisperse star chains have considerably small $\varphi'(t)$ in the terminal regime,[14] as similar to the situation for the blends examined in this study. Thus, the tube-edge fluctuation should also have an important effect on the slow dynamics of the star chains, in contradiction to a recent question[40] posed on this effect.

MA030443Y